

**UCLA**

**UCLA Electronic Theses and Dissertations**

**Title**

Sensorized Silicone Transfemoral Model Limbs

**Permalink**

<https://escholarship.org/uc/item/46d5k2pr>

**Author**

Khatibi, Amin Ebrahim

**Publication Date**

2024

Peer reviewed|Thesis/dissertation

UNIVERSITY OF CALIFORNIA

Los Angeles

Sensorized Silicone Transfemoral Model Limbs

A thesis submitted in partial satisfaction  
of the requirements for the degree  
Master of Science in Mechanical Engineering

by

Amin Ebrahim Khatibi

2024

© Copyright by

Amin Ebrahim Khatibi

2024

## ABSTRACT OF THE THESIS

Sensorized Silicone Transfemoral Model Limbs

by

Amin Ebrahim Khatibi

Master of Science in Mechanical Engineering

University of California, Los Angeles, 2024

Professor Tyler R. Clites, Chair

The UCLA Anatomical Engineering Group has developed an innovative attachment method for prosthetic sockets using an implantable ferromagnetic element and an externally controlled electromagnet to connect the socket to the limb. As part of this project, it was crucial to construct sensorized silicone limb models to effectively compare the new attachment method with conventional ones. These limb models also serve to validate various socket types, such as ischial containment sockets or quadrilateral sockets.

To design the limb models, the team used a 3D scan of an actual patient's limb, provided by the Veterans Affairs (VA) Medical Center, ensuring anatomical accuracy. The bone model within the limb was precisely sized and positioned using X-ray data, which informed the design's structural elements. The limb models were embedded with piezoelectric (PZT) crystals to measure

localized tissue deformation through sonomicrometry, a technique that uses acoustic signals to determine distances between crystals.

The construction phase involved 3D printing with advanced materials to create anatomically accurate limb models. The inclusion of pressure and temperature sensors allowed for comprehensive data collection on the limb's response during movement. An important aspect of the design was to account for volume changes, as an amputee's limb volume can vary throughout the day due to factors such as diet, weather, and comorbidities. Different mold sizes were constructed to test the same limb geometry at different volumes, ensuring the attachment method's effectiveness under varying conditions.

The sensorized limb models were tested and validated using various methods. Sonomicrometry was calibrated using water tests, while pressure sensors were individually calibrated and tested to ensure accurate measurements. Each limb model cost approximately \$1,720 without the ferromagnetic implant and \$2,100 with the implant. The final weight of the device was 17.4 pounds (7.89 kg). Future work involves collaboration with the UCLA Prosthetics and Orthotics Rehabilitation Center to create custom check sockets and further testing with the KUKA robot to simulate gait cycles. This multidisciplinary approach aims to set a new standard in prosthetic limb development, ultimately enhancing the fit, comfort, and quality of life for amputee patients.

The thesis of Amin Ebrahim Khatibi is approved.

Xiaochun Li

Jonathan Hopkins

Tyler R. Clites, Committee Chair

University of California, Los Angeles

2024

## **Dedication page**

To my family, whose unwavering support and encouragement have been instrumental in completing this project. Their belief in me has been a constant source of motivation throughout my academic journey.

To my friends and lab members, who have provided me with companionship, assistance, and moral support during the challenging times. Their understanding and encouragement have been invaluable.

To my professors, whose guidance and expertise have been crucial to my academic development. Their mentorship has contributed to my growth as a scholar.

To UCLA, for providing the resources and environment that have enabled me to complete this project. The opportunities and support offered by this institution have been essential to my success.

## Table of Contents

1	Introduction.....	1
2	Background & Motivation .....	4
2.1	Background.....	4
2.2	Motivation.....	7
3	Design.....	8
3.1	Preliminary Design .....	8
3.1.1	KUKA Attachment .....	10
3.1.2	Limb Profile.....	12
3.1.3	Bone STL with Aluminum Tube .....	13
3.1.4	Sensor Selection.....	14
3.1.5	Mold Design.....	16
3.1.6	Discussion: Preliminary Design.....	17
3.2	Secondary Design .....	19
3.2.1	KUKA Attachment .....	20
3.2.2	Limb Profile.....	21
3.2.3	New Bone Design .....	23
3.2.4	Sensor Selection.....	25
3.2.5	Mold Design.....	28
3.2.6	Discussion: Secondary Design.....	31
3.3	Final Design .....	33
3.3.1	KUKA Attachment .....	34
3.3.1.1	KUKA Attachment Design.....	34
3.3.1.2	KUKA Attachment FEA Validation.....	35



3.3.2	Limb Shape .....	38
3.3.3	Bone Design.....	40
3.3.3.1	Aluminum Tube .....	41
3.3.3.2	Bone Cover Final Design.....	44
3.3.3.3	Distal Femur Bone Model.....	47
3.3.4	Sensor Selection.....	48
3.3.4.1	Sonomicrometry.....	49
3.3.4.2	Pressure & Temperature Sensors .....	55
3.3.4.3	Wire Grommet Design .....	56
3.3.5	Mold Design.....	58
3.3.6	Discussion: Final Design .....	60
4	Construction.....	62
4.1	KUKA Attachment Construction.....	62
4.2	Model Bone Construction.....	63
4.2.1	Bone Cover Construction.....	64
4.2.2	Aluminum Tube Construction .....	65
4.3	Sensor Construction .....	66
4.4	Mold Construction .....	69
4.4.1	3D Printing (-10% Volume, Nominal, +10% Volume).....	69
4.5	Sensor Wiring .....	72
4.6	Sensor Pre-Molding .....	75
4.7	Final Molding Process .....	77
4.8	Construction Discussion .....	84
5	Validation.....	86

5.1	Silicone Validation.....	86
5.2	Volume Change Validation.....	88
5.3	Sonomicrometry Device Calibration in Silicone .....	90
5.4	Water Test.....	91
5.5	Sono & Final Device Validation.....	97
5.6	Pressure Sensor Validation .....	102
5.6.1	Distal Femur Pressure Sensor .....	102
5.6.2	Greater Trochanter Pressure Sensor.....	103
5.6.3	Ischial Tuberosity Pressure Sensor .....	103
5.6.4	Temperature Measurement .....	104
5.7	Validation Discussion .....	106
6	Conclusion & Future Work.....	108
6.1	Conclusion .....	108
6.2	Future Work .....	109
7	Appendix.....	111
8	References.....	119

## List of Figures

<b>Figure 1:</b> The UCLA Anatomical Engineering Group’s Magnetic Attachment Project. [2].....	1
<b>Figure 2:</b> A 6-Axis Industrial Robot with a sensorized model limb attached to the end effector. [2].....	2
<b>Figure 3:</b> The Anatomical Engineering Group’s sensorized silicone limb design. The ischial tuberosity and greater trochanter are marked with red and blue circles, respectively. The green circle represents the distal femur.....	4
<b>Figure 4:</b> A diagram showing the pressure-sensitive and pressure-tolerant areas of a transfemoral stump. The greater trochanter is in the pressure-sensitive section, while the ischial tuberosity is in the pressure-tolerant section. Most prosthetic socket types focus the load on the pressure-tolerant section to increase comfort for the user [4].....	5
<b>Figure 5:</b> Preliminary Design of the model limb with the ferromagnetic implant.....	8
<b>Figure 6:</b> Existing KUKA infrastructure in the lab (left). Initial attachment design (right).....	10
<b>Figure 7:</b> New KUKA mount infrastructure made by a different lab member (left). New design that utilizes fasteners to attach the limb to the KUKA robot (right).....	11
<b>Figure 8:</b> Preliminary model limb design. ....	12
<b>Figure 9:</b> Bone model with implemented aluminum tube utilized for strength.....	13
<b>Figure 10:</b> Initial sensor experiments using black silicone rings and piezoelectric bend sensors on a half-scale limb. ....	15
<b>Figure 11:</b> Preliminary single piece mold design utilized to construct the 1/2 scale limb. ....	16
<b>Figure 12:</b> Secondary Design Overview.....	19
<b>Figure 13:</b> KUKA attachment method using two M10 bolts to connect to the model bone and 6 M10 bolts to connect to the KUKA infrastructure.....	20
<b>Figure 14:</b> Transfemoral amputee patient's limb 3D scan. Unmodified limb profile (left). Modified Limb profile with colored lines representing the modification method (middle). Ischial tuberosity hard stop location represented with the blue dot (right).....	21
<b>Figure 15:</b> The Limb Model created using the STL file provided by the VA. The limb was split into 12 equally spaced sections which can be seen by the splines.....	22
<b>Figure 16:</b> Published X-ray data [8] [9] used to validate the model bone size. The model bone was aligned using the frontal plane (left/ middle image) and then also oriented using the side view (right).....	23

<b>Figure 17:</b> Secondary bone design modeled based on published X-ray Data. The two holes are utilized to connect the model bone to the aluminum tube. ....	24
<b>Figure 18:</b> 8-Channel sonomicrometry device that was rented from Sonometrics.....	25
<b>Figure 19:</b> Initial sensor placement concept for the sonomicrometry system. Red crystals represent the 2mm sonomicrometry crystals. ....	26
<b>Figure 20:</b> Secondary half-scale design with implanted sonomicrometry sensors.....	27
<b>Figure 21:</b> Three-piece mold designed to ease bone placement and part removal. ....	28
<b>Figure 22:</b> 1/2 Scale 3D printed mold design (orange) with the bone alignment tool (white). ...	29
<b>Figure 23:</b> Various methods of improving the mold surface quality. 2 in 1 sandable primer (left), glazing spot putty (middle), sanding (Right). ....	29
<b>Figure 24:</b> Final Design renderings with (left) and without (right) the ferromagnetic implant...	33
<b>Figure 25:</b> KUKA Attachment method final design. ....	34
<b>Figure 26:</b> Mesh design for the FEA analysis of the KUKA attachment device. ....	36
<b>Figure 27:</b> Von Mises stress analysis. The peak stress was $5.224 \times 10^7$ N/m <sup>2</sup> , and the yield strength was $5.515 \times 10^7$ N/m <sup>2</sup> . The deformation is exaggerated for visual purposes.....	36
<b>Figure 28:</b> Motion Study Displacement plot. The maximum displacement occurs towards the edge of the plate with a value of 0.4792 mm under the 1000N load. This figure is exaggerated for visual purposes. ....	37
<b>Figure 29:</b> Strain plot from the motion study. The maximum strain is $6.715 \times 10^{-4}$ mm at the red locations. The figure is exaggerated for visual purposes ....	37
<b>Figure 30:</b> Modified limb profile to better cover the pelvis and provide a minimum tissue thickness of 15 mm around the implant. Frontal view (Left), Side view (Middle), locations of the edit represented by the red circles (Right). ....	38
<b>Figure 31:</b> Bone design for the case with an implant (left) and without an implant (right). ....	40
<b>Figure 32:</b> Aluminum tube design with various hole sizes and locations. The sensor wires will enter the tube from the slot location (green) and exit throughout the limb at the designated locations (red). ....	41
<b>Figure 33:</b> SolidWorks Simulation von Mises stress plot. The maximum stress was $8.573 \times 10^6$ N/m <sup>2</sup> , and the yield strength was $5.515 \times 10^7$ N/m <sup>2</sup> . The peak stress is experienced at the holes designed for wiring towards the bottom of the limb. The figure is exaggerated for visual purposes. ....	42

**Figure 34:** SolidWorks displacement plot. The maximum displacement at the distal end of the bone was 0.02133 mm. This figure is exaggerated for visual purposes. .... 43

**Figure 35:** The SolidWorks strain plot. The location of the maximum strain is similar to the location of the maximum stress, which is near the holes designed for the wiring. This figure is exaggerated for visual purposes. .... 43

**Figure 36:** Finalized model bone cover design. The location of the three standoffs used to ground the sono crystals is shown by the red circles. The location of the threaded inserts is represented by the green circle..... 44

**Figure 37:** Model bone mesh design. The force is applied on the ischial tuberosity, which is the hard stop used for ischial containment sockets. The green arrows represent the grounding location..... 45

**Figure 38:** SolidWorks simulation stress plots. The maximum stress is experienced at the ischial tuberosity with a value of  $1.796 \times 10^8$  N/m<sup>2</sup>. The maximum strain value was  $8.047 \times 10^{-2}$ . This figure is exaggerated for visual purposes..... 46

**Figure 39:** SolidWorks simulation deformation plots. The maximum displacement is experienced at the ischial tuberosity with a value of 2.923 mm. .... 46

**Figure 40:** Distal femur bone model for the no implant case. .... 47

**Figure 41:** Final limb model with implemented sensors and wiring with(left) and without (right) the implant. .... 48

**Figure 42:** Digital 12-channel transceiver sonomicrometer hardware from SonoMetrics Corporation. An additional 12-channel breakout box is used to extend the sensors wire lengths. The device costs \$16,000, and the breakout box costs \$700..... 49

**Figure 43:** Close-up view of the grounded crystal design and position. Crystal 1 is the purple crystal on the right, crystal 2 is towards the bottom, and crystal 3 is on the top left of the figure. .... 50

**Figure 44:** Finalized crystal placement, demonstrating the strategic distribution and orientation of sono crystals on different levels of the limb for optimal data triangulation. The top box consists of crystals 5, 9, 11. The middle box consists of crystals 4, 6, 12. The bottom box consists of crystals 7, 8, 10. .... 52

<b>Figure 45:</b> Sonomicrometer breakout box KUKA attachment. The breakout box is fastened to this piece using screws and bolts. Once fastened, this part secures to the KUKA with Velcro straps. ....	54
<b>Figure 46:</b> The 16 pressure sensors' locations relative to the sono crystal placement. Three of the pressure sensors are on the back side of the limb and are not visible.....	55
<b>Figure 47:</b> 3D grommet design which prevents damage to the cables. ....	57
<b>Figure 48:</b> Isometric (left) and side view (right) of the final mold design. The top piece surrounded by the red box is the limb alignment device used to position the model bone within the limb. The piece surrounded by the green box is used to connect the top and bottom halves of the mold.....	58
<b>Figure 49:</b> The machined KUKA attachment. ....	62
<b>Figure 50:</b> Model bone construction for the case with the ferromagnetic implant.....	63
<b>Figure 51:</b> Markforged Mark 2, 3D printer with the pelvis printed with Onyx.....	64
<b>Figure 52:</b> Machined aluminum tube with the various components and fasteners needed to assemble the bone model for the case with the implant.....	65
<b>Figure 53:</b> The tin stencil used to apply solder paste to the PCB prior to installing the components (left). The PCB board for 10 pressure sensors with the applied solder paste (right). ....	66
<b>Figure 54:</b> The 10 completed pressure sensors with two resistors, one capacitor, and one pressure sensor that were installed prior to being placed in the oven for the solder's melting. ....	67
<b>Figure 55:</b> The reflow used to heat the solder paste to 170°C.....	67
<b>Figure 56:</b> The 16 finalized pressure sensors with the shielded wiring installed. ....	68
<b>Figure 57:</b> The Dremel 3D45 used to print the mold and bone alignment parts. ....	69
<b>Figure 58:</b> The Bone alignment part that was printed using Eco ABS filament on the Dremel 3D45.....	70
<b>Figure 59:</b> A comparison of the 3D printed part without (left) and with (right) the XTC-3D finish. ....	71
<b>Figure 60:</b> The sono ground crystals 1,2, and 3 (highlighted by the red circles) were the first to be installed; these crystals were tested in water to confirm their functionality. ....	72

<b>Figure 61:</b> The 16 pressure sensors and 12 sono crystals that were successfully routed through the molded bone. ....	73
<b>Figure 62:</b> Pre-molded sonomicrometry and pressure sensors with the silicone poured into the molds. ....	75
<b>Figure 63:</b> The sensors encased in silicone prior to the final molding prosses. ....	76
<b>Figure 64:</b> The final molding of the limb was divided into 10 separate pours, selected based on component positioning and the maximum recommended amount of poured silicone. ....	77
<b>Figure 65:</b> The initial 200-gram silicone pour preventing wires from sticking through the bottom of the limb. ....	78
<b>Figure 66:</b> The stencil used to position crystals 7, 8, and 10 with their respective pressure sensors on the bottom level of the limb. ....	79
<b>Figure 67:</b> The first two levels of silicone with the bottom level of pressure sensors and sono crystals embedded. ....	79
<b>Figure 68:</b> The removable template used to position sensors at the correct level, prepared for the 4th pour. ....	80
<b>Figure 69:</b> Mid-level sensors with silicone poured to the top of level 5 in preparation for level 6. ....	80
<b>Figure 70:</b> The final molding result with 7450 grams of cured silicone poured in ten sections..	81
<b>Figure 71:</b> The demolding process, with the top sections removed first to avoid damaging the mold or silicone limbs. ....	82
<b>Figure 72:</b> The final sensorized model limb with the KUKA attachment mounted. The red circles highlight the implanted pressure and sono crystals on this side of the limb. ....	83
<b>Figure 73:</b> The various silicones tested for the limb from left to right: Dragon Skin 10, Ecoflex Gel 2, Ecoflex 00-20, Ecoflex 00-31 Near Clear, and Ecoflex 00-45 Near Clear. ....	87
<b>Figure 74:</b> The 3D printed molds with three different inner volumes: -10%, nominal, +10%....	88
<b>Figure 75:</b> The apparatus used to calibrate the sonomicrometry device to the Ecoflex 00-31 silicone. ....	90
<b>Figure 76:</b> The sono water test model used to validate the crystal placement. Three crystals are grounded, and nine crystals are attached to their respective connectors, representing the wire length. ....	91

<b>Figure 77:</b> The sono water test experimental setup, including the breakout box and attachment, the KUKA attachment device, the model bone, and the aluminum tube and bone cover. ...	92
<b>Figure 78:</b> The XYZ coordinates from the CAD (pink stars) plotted against the results from the sonomicrometry triangulation test in water (blue dots). .....	93
<b>Figure 79:</b> The distance between the actual location and the designed location for each crystal. ....	93
<b>Figure 80:</b> The movement of crystals 11, 5, and 9. ....	94
<b>Figure 81:</b> A close-up of moving only crystal 11, showing the remaining crystals stationary with no movement. ....	95
<b>Figure 82:</b> The final image with the sensorized model limb attached to the six-axis KUKA robotic arm. ....	97
<b>Figure 83:</b> A close-up view of the breakout box (left) and sensorized model limb (right) attached to the end effector of the KUKA robotic arm. ....	98
<b>Figure 84:</b> The XYZ coordinates from the CAD (pink stars) plotted against the results from the sonomicrometry triangulation test in silicone (blue dots) in 3D. ....	99
<b>Figure 85:</b> The distance between the actual location and the designed location for each crystal. The average difference is less than 5mm, which is remarkable considering the overall size of the limb. ....	99
<b>Figure 86:</b> The movement of crystals 4-12 in millimeters vs. time. In this experiment, only the location of crystal 8 was pressed. ....	100
<b>Figure 87:</b> The plot of movement in millimeters vs time when placing a 25-pound weight on top of the limb and removing it three times, indicated by the three distinct curves. ....	101
<b>Figure 88:</b> The pressure vs. time plot of the distal femur created by pressing the end of the bone five times. The maximum recorded pressure was 10543.4 Pa. ....	102
<b>Figure 89:</b> The pressure at the greater trochanter created by pressing and releasing the greater trochanter five times. The maximum recorded pressure was 8507.9 Pa. ....	103
<b>Figure 90:</b> The pressure at the ischial tuberosity created by pressing and releasing this bony landmark five times. The maximum recorded pressure was 7980.3 Pa. ....	104
<b>Figure 91:</b> The temperature of the distal femur recorded while completing the pressure experiment. The maximum recorded temperature was 22.2o Celsius. ....	104



**Figure 92:** The initial stages of making a check socket for the sensorized silicone limb model detailed in this report. The UCLA Prosthetics and Orthotics Center has created a limb positive of our model limb in preparation to build the check socket. .... 109

**Figure 93:** The KUKA Attachment device engineering drawing sent to SuNPe for machining. .... 111

**Figure 94:** Engineering drawing of the aluminum tube used at UCLA machine shop to make the model..... 112

**Figure 95:** The SonoMetrics Quote for the 12 channel sonomicrometer. .... 114

**Figure 96:** The SonoMetrics quote for the breakout box and eight 2mm transducer on silastic tubing. .... 115

**Figure 97:** The quote from Reynolds Advanced Materials for a 5-gallon unit of Ecoflex 00-31 Near Clear. .... 116

**Figure 98:** The Mechanical and Aerospace Engineering PAC order form for the BVV vacuum chamber..... 117

**Figure 99:** The prototyping quote from SuNPe for the KUKA attachment device. .... 118

## **Acknowledgments**

I would like to express my sincere gratitude to Mr. Will Flanagan for his invaluable assistance and contributions throughout this project. Special thanks to Dr. Tyler Clites for his guidance and mentorship, which were instrumental in the completion of this work.

This work was supported in part by the U.S. Department of Defense under Grant W81XWH2220046.

# 1 INTRODUCTION

---

The UCLA Anatomical Engineering Group is pioneering an innovative project focused on developing an electromagnetic attachment system for prosthetic limbs; this system seeks to connect a ferromagnetic implant directly to the bone, using an external electromagnet to attach the prosthetic socket to the limb (see **Figure 1** below). The attachment design's primary benefit results from directly transferring the applied load to the bone, which minimizes the pistoning effect associated with traditional soft tissue attachment methods. Pistoning, defined as the vertical displacement of the limb within the prosthetic socket, is a significant challenge in conventional prosthetic fittings [1].

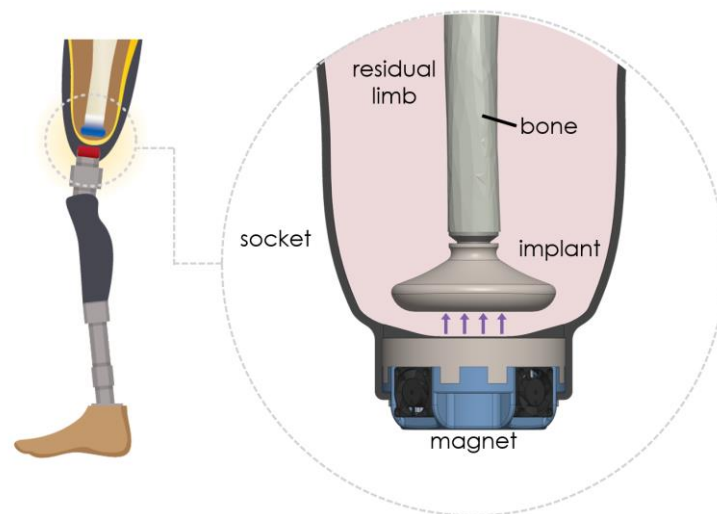


*Figure 1: The UCLA Anatomical Engineering Group's Magnetic Attachment Project. [2]*

To validate the feasibility of the design, the team will test this system during gait and compare the results with conventional suspension methods. Utilizing a 6-axis industrial robot to simulate the gait cycle (see **Figure 2** below), the team's objective is to design sensorized silicone model limbs capable of measuring various parameters, including temperature, pressure, and local tissue deformation. Local tissue deformation refers to the movement of soft tissue around the limb

relative to the bone. These sensorized limbs will allow for the refinement of prosthetic device design and control based on precise data.

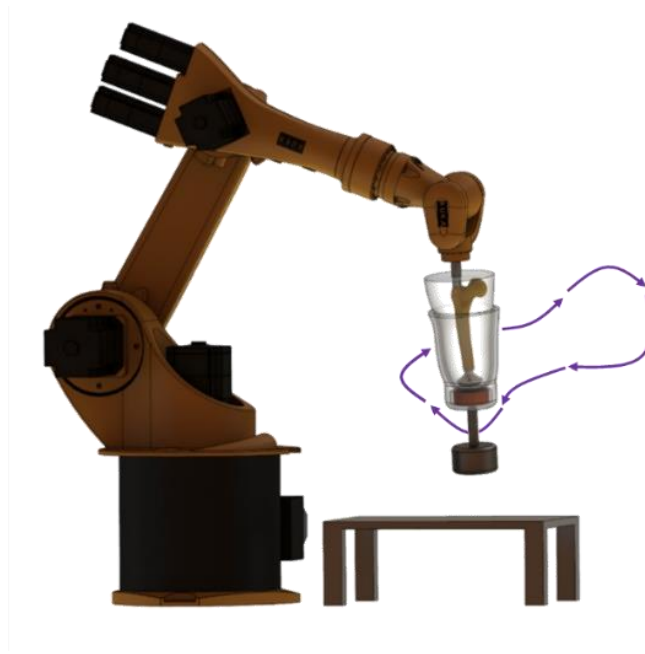


*Figure 2: A 6-Axis Industrial Robot with a sensorized model limb attached to the end effector. [2]*

The team's research involves embedding piezoelectric (PZT) crystals into the silicone limbs to measure localized tissue deformation. The KUKA robotic arm's movements induce deformation in the model tissue, moving the PZT crystals. By employing sonomicrometry, the team seeks to analyze the impact of magnetic attachment versus traditional socket attachment methods. Doing so will yield data on how different attachment methods affect tissue deformation and overall limb dynamics.

This project collaborates with the Veterans Affairs (VA) Medical Center in Westwood and the UCLA Prosthetics and Orthotics facility; said collaborations were vital in securing critical components such as scanned limb models and prosthetic sockets.

The team believes in the necessity of creating a standardized device for developing new prosthetic technologies. The goal of this project is to create a model limb that is illustrative of an

actual patient's residual limb. Once constructed, these limb models will be taken to the VA for verification and later to build suitable prosthetic sockets.

This report focuses on three key aspects of the sensorized limb project. First, the design phase, which details the choice of materials and various design elements. Second, the construction phase of the sensorized limbs, which explains the meticulous process of assembling the components and integrating the sensors. Lastly, the validation phase, which demonstrates that the model limbs function as intended and justifies the choices made throughout the project.

## 2 BACKGROUND & MOTIVATION

---

### 2.1 BACKGROUND

Traditionally, researchers have relied on cadaver limbs for prosthetic development. Despite its effectiveness, the variability between cadaver limbs presents significant challenges in standardizing prosthetic designs. As a result, extensive research has focused on developing sensorized model limbs, which allow for the creation of a universal standard for prosthetic limbs. Establishing such a standard is crucial for quantifying the comfort and usability of prosthetics, thereby enabling more consistent and reliable advancements in prosthetic technology.

Sensorized limbs are designed to measure three types of data at key anatomical landmarks: localized tissue deformation, temperature, and mechanical forces. These landmarks include the ischial tuberosity, greater trochanter, and distal femur, as depicted in **Figure 3** below.



*Figure 3: The Anatomical Engineering Group's sensorized silicone limb design. The ischial tuberosity and greater trochanter are marked with red and blue circles, respectively. The green circle represents the distal femur.*

The ischial tuberosity, also known as the "sitting bone," is a crucial bony landmark that bears the body's weight when sitting. Several important soft tissue structures attach to this tuberosity, including the Sacro tuberos ligament, some gluteal muscles (inferior gemellus, quadratus femoris), adductor magnus, and the posterior thigh muscles (biceps femoris, semitendinosus, semimembranosus). The ischial tuberosities serve as landmarks for dividing the perineum into the anterior urogenital triangle and the posterior anal triangle and help locate the sciatic nerve, which descends through the pelvis between the ischial tuberosity and the greater trochanter of the femur [3]. Understanding the forces exerted at this bony landmark is indispensable to guarantee the comfort of the prosthetic socket for patients when sitting or moving.

Another critical bony landmark is the greater trochanter. Most prosthetic sockets are designed to cover the greater trochanter to help distribute the load. The position of the greater trochanter affects the mechanical stress on the hip joint, the extent of contraction of the gluteus medius and minimus muscles, and the mechanical stress on the femoral neck [4].

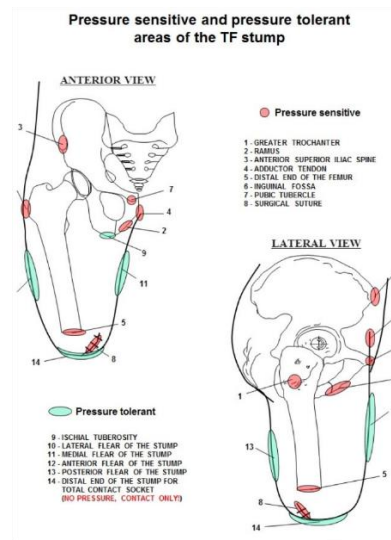


*Figure 4: A diagram showing the pressure-sensitive and pressure-tolerant areas of a transfemoral stump. The greater trochanter is in the pressure-sensitive section, while the ischial tuberosity is in the pressure-tolerant section. Most prosthetic socket types focus the load on the pressure-tolerant section to increase comfort for the user [5].*

**Figure 4** above illustrates the pressure-sensitive and pressure-tolerant areas of the transfemoral stump. The greater trochanter is pressure-sensitive, while the ischial tuberosity is pressure-tolerant. Consequently, some prosthetists prefer using an ischial containment socket, which places more of the load on the ischial tuberosity to increase the patient's comfort.

There are two main types of sockets for transfemoral (above-the-knee) amputees: (1) quadrilateral and (2) ischial containment. Quadrilateral sockets use opposing forces to hold the residual limb in position, ensuring the ischial tuberosity remains on the seating area on the posterior of the socket; these sockets are better suited for individuals with lower activity levels and/or longer residual limbs. On the other hand, ischial containment sockets contain the ischium within it, supporting the ischium and ramus medially while holding the femur in position; this design creates a bony lock, providing greater control within the socket and is suitable for a wide variety of users, including those who are very active and/or have short and fleshy residual limbs [6].

There is no definitive choice for a patient who is selecting their prosthetic socket. Each prosthetist may recommend a different socket type as the "best fit", with various justifications for their selection. The goal of this research is to construct a device that can compare different socket types to determine which is most comfortable and why; this will be achieved by analyzing the load on the bony landmarks mentioned above and the pressure distributions throughout the soft tissue.



## 2.2 MOTIVATION

The motivation behind this research stems from the need to address common issues faced by prosthetic users. Most prosthetic users do not struggle with the complexity of their devices; instead, they face challenges related to fit and comfort. An ill-fitting socket can lead to serious complications such as redness, blistering, and ulcers, particularly for lower limb amputees [7]. These issues are further exacerbated by muscle atrophy, which can cause painful socket pistoning.

By developing a sensorized model limb, the team aims to better understand the forces and pressure distributions across a residual limb; this understanding will allow for designing prosthetic sockets that offer improved fitment and comfort [8]. The goal is to create a standardized model that can be used to develop new prosthetic technologies, which enhances the quality of life for amputee patients.

By integrating advanced sensing technologies and innovative attachment methods, the team hopes to set a new standard for prosthetic limb development. The insights gained from this research will contribute to the creation of prosthetic devices that are functional and significantly more comfortable for users.

### 3 DESIGN

---

#### 3.1 PRELIMINARY DESIGN

To begin designing the model limb, the team discussed various design elements that had to be followed. First, the limb had to resemble that of a 100 kg (about 220.46 lb.) subject. Second, it was essential for the limb to look anatomically correct. Third, the design needed to be compatible with the existing infrastructure to minimize potential implementation issues. **Figure 5** below shows a rendering of the preliminary design.



*Figure 5: Preliminary Design of the model limb with the ferromagnetic implant.*

The design process started with obtaining an STL file of a model femur and pelvis. Using simple beam bending calculations, an aluminum rod was selected that could withstand the bending forces due to the applied loads. Additionally, we determined the rough diameter of a 100 kg person's quadriceps. With these parameters, the theoretical shape of the limb was modeled, and the outer profile of the design was defined. The implant, designed by another lab member, was then incorporated into this limb, with its top attached to the selected aluminum rod. Finally, using the theoretical outer profile of the model limb, a potential prosthetic socket was modeled.

### 3.1.1 KUKA Attachment

The model limb was designed to be friction-mounted to the KUKA robotic system. The initial plan involved manufacturing the model bone using bone cement to pot a mold that would fit into the existing KUKA mount. This approach required modifying the pelvis to ensure proper fitment of the limb. The design leveraged the existing infrastructure in the lab to expedite testing and integration.

The figure below shows the existing infrastructure created by previous lab members on the left and the preliminary design on the right. The design aimed to integrate seamlessly with this setup, allowing for immediate testing and validation of the model limb.

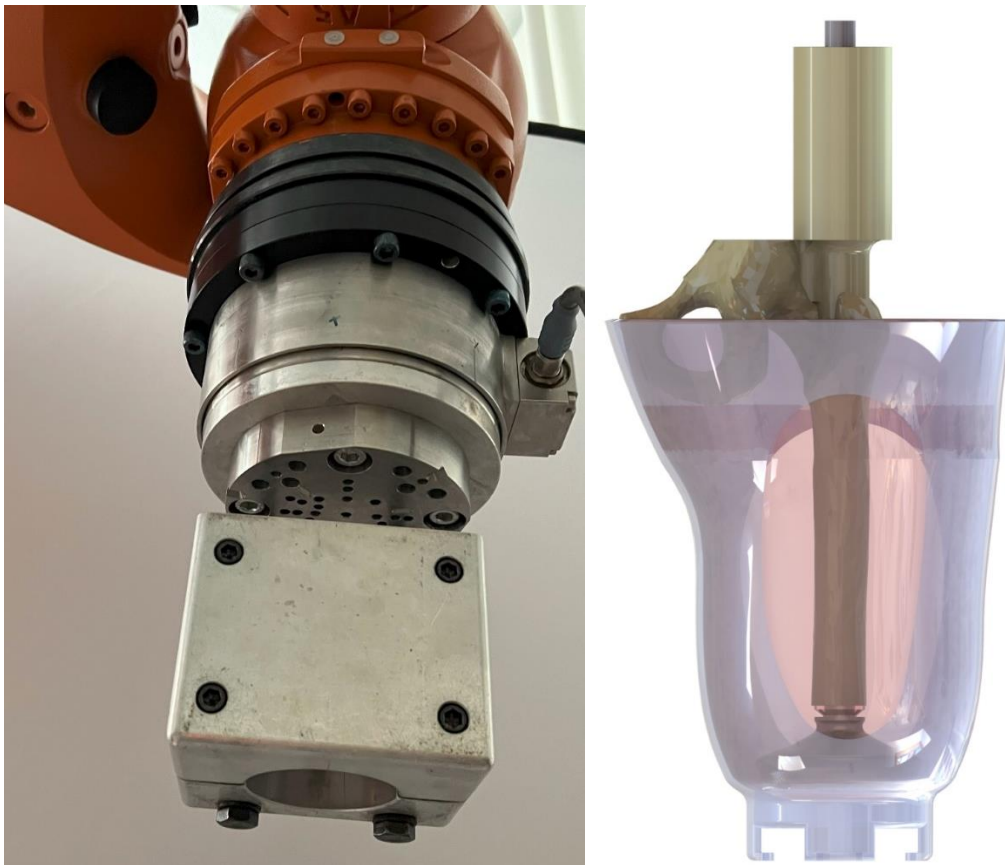


*Figure 6: Existing KUKA infrastructure in the lab (left). Initial attachment design (right).*

However, after the lab upgraded the KUKA attachment infrastructure (**Figure 7**), the team pursued a more robust design that was mechanically fastened to the KUKA. This new approach allowed the application of significantly more force to the design without the possibility of limb failure. The new design, created by one of the current lab members, is backwards compatible with previous designs but offers more attachment methods for various devices. This enhanced flexibility and robustness ensures better performance and reliability under higher loads.

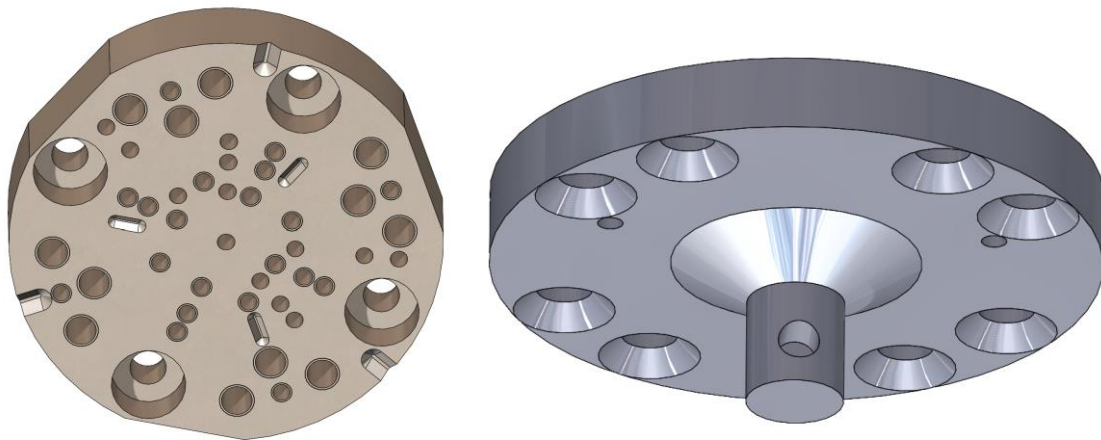


*Figure 7: New KUKA mount infrastructure made by a different lab member (left). New design that utilizes fasteners to attach the limb to the KUKA robot (right).*

The new KUKA attachment method utilized eight countersunk M10 by 30mm bolts to connect to the KUKA infrastructure, and one M10 by 40mm bolt and nut to connect the model bone to the KUKA. Additionally, it features two alignment pins to ensure precise alignment relative to the KUKA end effector. This design aimed to provide a more robust connection, allowing for the application of significantly more force without the risk of limb failure.

### 3.1.2 Limb Profile

The initial outer limb shape was created by examining X-ray images and photographs of transfemoral amputee patients' limbs. This approach allowed the team to model a theoretical limb based on anatomical references. Hypothetical splines were made at specific limb levels, which were then lofted in SolidWorks using the lofted boss feature. This process resulted in an initial limb shape, which was instrumental in explaining the design to the VA and other interested parties.

**Figure 8** below shows the preliminary model limb design.



*Figure 8: Preliminary model limb design.*

### 3.1.3 Bone STL with Aluminum Tube

To design the model bone, an STL file of the femur and pelvis was imported into SolidWorks and converted to a part file. Using this part file, the model bone was modified, and an aluminum rod was selected to be inserted into the bone to strengthen it, ensuring it could withstand the loads present during gait. Initially, the design aimed for the limb to resemble an actual patient's residual limb, including the upper pelvis. However, after further consideration, the design was simplified to focus on the more crucial parts of the limb. This simplification involved cutting the pelvis and redesigning the attachment methods for the second version of the model limb.

In the initial design, the bone and aluminum rod were positioned vertically, minimizing the chance of the smaller rod breaking or bending under the load. This design served as adequate proof of concept. However, it was significantly modified to better align with the vision for sensorized silicone limbs. The aluminum tube was used to strengthen the bone and facilitate the attachment of the implant (**Figure 9**).

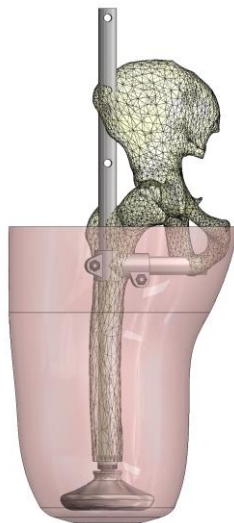


*Figure 9: Bone model with implemented aluminum tube utilized for strength.*

### 3.1.4 Sensor Selection

To sensorize the model limb, the team constructed a 1/2 scale version to validate the limb shape, model bone, and implant attachment method. Initially, the team experimented with a few methods to measure movement throughout the limb.

The first approach involved implanting black silicone rings inside the limb where the soft tissue would be. These rings were placed 15mm apart and molded layer by layer. The intention was to use a high-speed camera to track the movement of these rings, allowing for the calculation of limb movement. However, this method required the use of clear sockets, and it proved challenging to accurately locate the silicone rings within the limb during movement.

The second approach involved using piezoelectric bend sensors. The resistance value of these sensors would change depending on how much they were bent. After implementing these sensors in the 1/2 scale limb, the team noticed a few issues. Firstly, the sensors were not as accurate as required. Secondly, the sensors would drift. Sensor drift refers to the phenomenon where the starting value of the sensors tends to increase, even when the limb or sensor is not experiencing any movement. **Figure 10** shows the model limb with the rings and sensors.



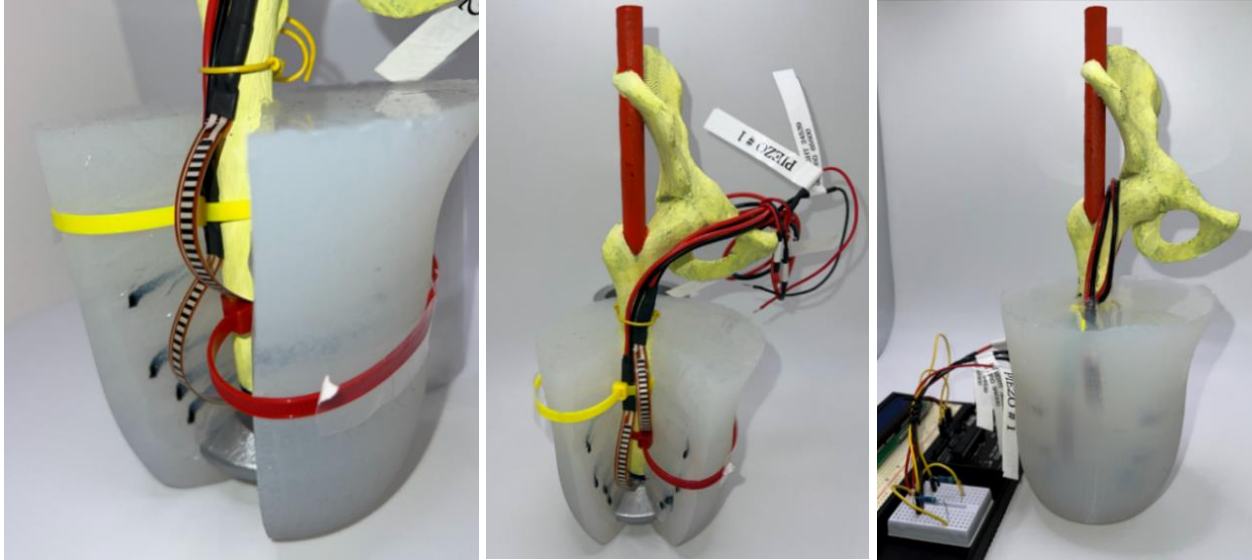


*Figure 10: Initial sensor experiments using black silicone rings and piezoelectric bend sensors on a half-scale limb.*

This experiment taught the team two crucial lessons. Firstly, creating the limb in individual layers was effective because the silicone would bind to itself, rendering the layers indistinguishable from one another, provided the limb was kept clean and free of oil or mold release material. Secondly, the sensor wires could be utilized as a web-like structure to secure the silicone to the bone, preventing the silicone from sliding off the end of the limb.

### 3.1.5 Mold Design

The primary goal of this mold was to test the silicone pouring method and determine whether a vacuum chamber was necessary. Additionally, the team aimed to explore the possibilities of 3D printing molds and molding them in stages within the limb. After completing the molding process, it became apparent that the mold design and molding conditions needed significant adjustments to accommodate a complex sensorized design.

Using a single-piece mold presented several challenges (**Figure 11**). It was very difficult to remove parts from the mold, and positioning sensors accurately within the mold proved to be impossible. Furthermore, the mold surface quality was very low, as the final molded limb exhibited layer lines from the 3D printing process. The silicone used in the model limb also had many air bubbles, which stressed the importance of a vacuum chamber for silicone molding. This process underscored the need for a more refined mold design and better molding conditions to achieve the desired theoretical limb profile.



*Figure 11: Preliminary single piece mold design utilized to construct the 1/2 scale limb.*

### **3.1.6 Discussion: Preliminary Design**

The preliminary design of the sensorized silicone model limb was instrumental in validating initial ideas and facilitating effective communication with the VA hospital regarding project requirements. By using this design, the team was able to acquire a 3D scan of an actual patient's limb from the VA hospital, ensuring that the model closely replicated the anatomical features of a real transfemoral amputee limb.

The design served as a proof of concept for the sensorized silicone limb. It allowed the team to explore various methods for sensor integration and to evaluate the feasibility of the proposed design. This initial phase was crucial in identifying key areas for improvement and setting the stage for more refined and functional prototypes.

It is important to note that we encountered salient issues during the preliminary design phase. The surface quality of the parts was poor because of the presence of layer lines from the 3D printing process. This affected the overall aesthetic and potentially the performance of the silicone limb. To address this, the mold design needed to be significantly refined to achieve a smoother and more accurate surface finish.

Another critical issue was the bone attachment to the KUKA. The initial design did not provide the robustness required for the loads experienced during gait. Consequently, the attachment method was redesigned to incorporate eight countersunk M10 by 30mm bolts for connecting to the KUKA infrastructure, along with one M10 by 40mm bolt and nut for attaching the model bone to the KUKA. Additionally, two alignment pins were added to ensure precise alignment with the KUKA end effector.

The mold design also required significant changes. The single-piece mold proved to be challenging for part removal and sensor positioning. The final molded limb exhibited layer lines from 3D printing and had numerous air bubbles, affecting the silicone's overall properties. This underscored the need for a more refined mold design and better molding conditions, potentially including the use of a vacuum chamber to eliminate air bubbles.

Furthermore, the sensor selection needed to be revisited. The initial experiments with black silicone rings and piezoelectric bend sensors revealed several limitations. The rings required clear sockets and were difficult to track accurately during movement. The piezoelectric bend sensors, while initially promising, exhibited drift and were not as accurate as needed. As a result, new sensor technologies and integration methods are being explored to enhance the accuracy and reliability of the sensorized silicone limb.

Overall, the preliminary design phase was essential in validating the initial concepts and identifying critical areas for improvement. The insights gained from this phase have guided the redesign efforts, ensuring that the next iterations of the model limb will be more robust, accurate, and functional. Continued collaboration with the VA hospital and iterative testing will be essential in achieving the project's goals and developing a highly effective sensorized silicone limb.

### 3.2 SECONDARY DESIGN

Utilizing the crucial concepts from the first design, the team decided to redesign every component to improve overall functionality while also adhering to better design practices. The goal was now to make a residual limb model that would more precisely represent an individual's residual limb. This redesigned model was more representative of the anatomical features and mechanical properties of a real limb. However, the bone component ended up being somewhat bulky to ensure it was strong enough to withstand a force of 1000N. **Figure 12** represents an overview of the secondary design iteration.

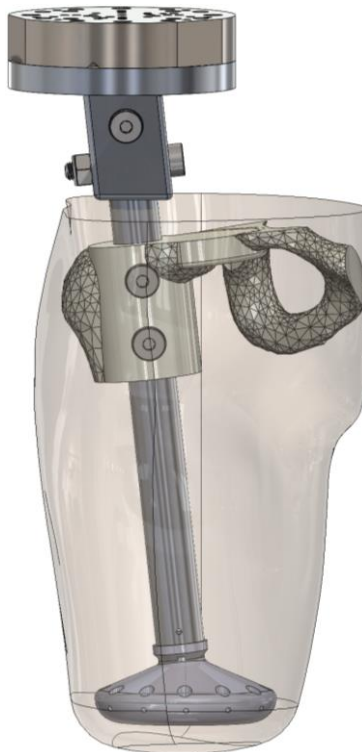


*Figure 12: Secondary Design Overview.*

### 3.2.1 KUKA Attachment

The KUKA attachment was redesigned to angle the bone at 6 degrees, because this design better matches anatomical models and more accurately represents the appearance of a person's limb and femur bone. However, this 6-degree angle introduced a few challenges. Firstly, it created a moment on the KUKA attachment, leading to potential failures. Secondly, it increased the bending moment exerted on the model bone. To address these issues, the team used Finite Element Analysis (FEA) to ensure the design was strong enough to withstand the anticipated forces.

The attachment featured two alignment holes to match the KUKA mount infrastructure described above. However, testing the 3D-printed version of this design revealed that it was over-constrained. Consequently, the design was revised once more for the final attachment method. The final KUKA mount was secured with six M10 bolts, which is sufficiently strong to hold the limb and withstand the loads generated by a 100kg person walking. This design also allowed the team to utilize two M10 bolts to connect the model bone to the KUKA mount, helping to distribute the load more evenly and prevent stress fractures on the model bone (**Figure 13**).

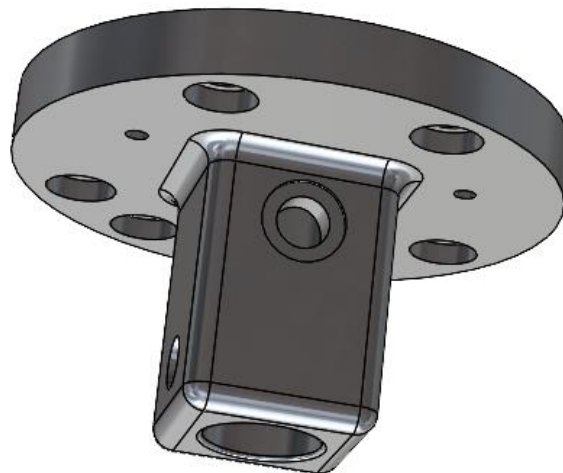


*Figure 13: KUKA attachment method using two M10 bolts to connect to the model bone and 6 M10 bolts to connect to the KUKA infrastructure.*

### 3.2.2 Limb Profile

After constructing the preliminary design model limb, the team presented the design at the West Los Angeles VA Medical Center and requested a 3D scan of an actual amputee patient's limb. The VA validated the design concept and provided the team with an unmodified limb scan. They also explained how they modify limb scans to design check sockets and where they place the hard stop for the socket. **Figure 14** below shows the unmodified limb, modified limb, and the hard stop location.

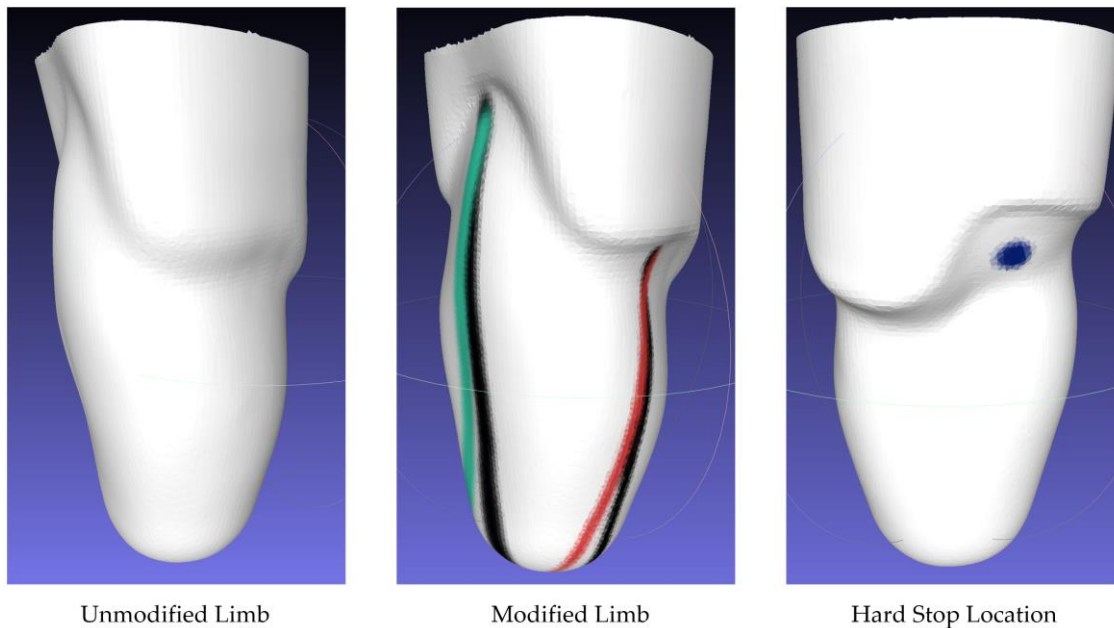


**Figure 14:** *Transfemoral amputee patient's limb 3D scan. Unmodified limb profile (left). Modified Limb profile with colored lines representing the modification method (middle). Ischial tuberosity hard stop location represented with the blue dot (right).*

Utilizing the limb scan obtained from the VA, we created a new outer profile. The bottom of the limb was cut to improve the overall limb shape and increase the cross-section to fit the implant. Using the STL file provided by the VA, the team constructed a SolidWorks part file by splitting the limb into 12 horizontal sections that were 3 cm apart. Using the spline feature, the team outlined the limb profile at each of the 12 sections and the outer profile of the limb to create

the guide curves for it. Then, using the “Lofted Boss/Base” feature, the team created a solid part file of the model limb; this is shown in **Figure 15** below. This limb profile was an accurate representation of the STL file provided by the VA, giving the team a starting profile of a transfemoral amputee patient's residual limb.

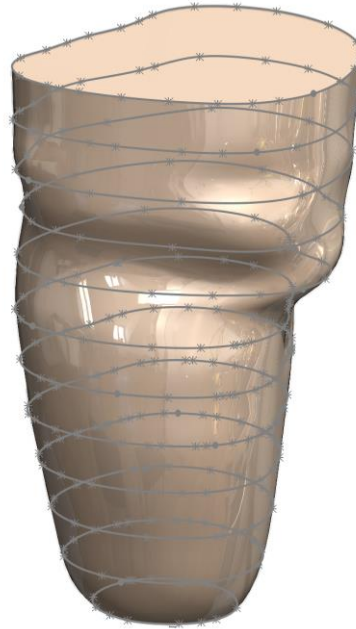


*Figure 15: The Limb Model created using the STL file provided by the VA. The limb was split into 12 equally spaced sections which can be seen by the splines.*



### 3.2.3 New Bone Design

Due to Institutional Review Board (IRB) restrictions, the team was unable to obtain the subject's X-ray data; the original plan was to use the X-ray data to better understand the bone size and location for the subject. To solve this problem, the team decided to use published X-ray data. **Figure 16** shows how the team sized the bone with the model limb. Using X-rays, the team determined the appropriate size of the bone for the subject and oriented the femur and pelvis to accurately match the data.

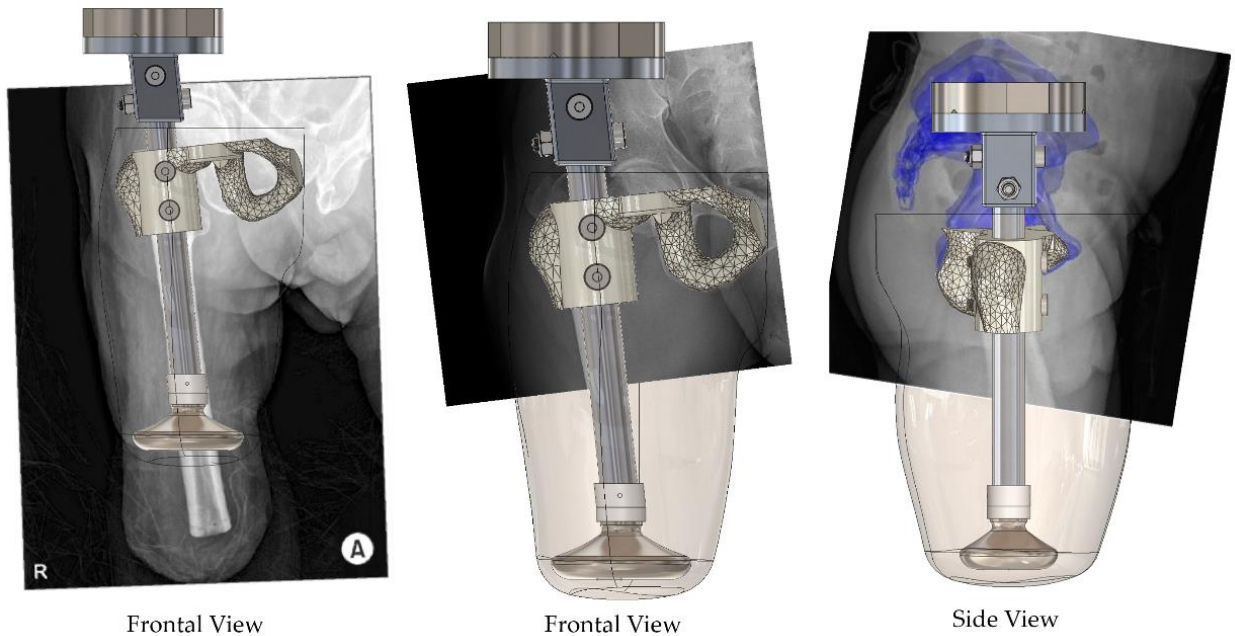


*Figure 16: Published X-ray data [9] [10] used to validate the model bone size. The model bone was aligned using the frontal plane (left/ middle image) and then also oriented using the side view (right).*

After appropriately sizing and orienting the bone, the team focused on making the bone stronger to withstand the 1000N load. This was achieved by adding material above the bone to minimize its effects on the components inside the simulated model limb. **Figure 17** depicts the modified bone design.

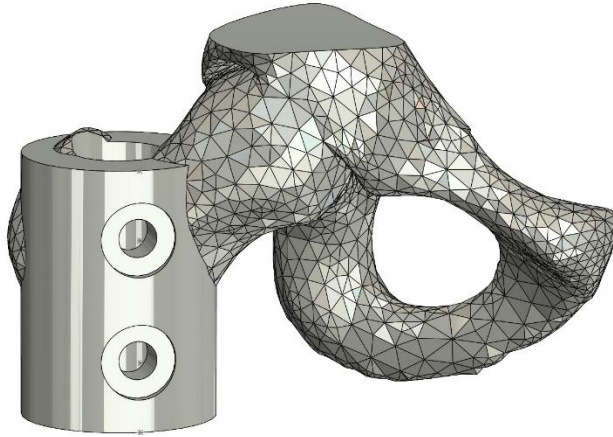


*Figure 17: Secondary bone design modeled based on published X-ray Data. The two holes are utilized to connect the model bone to the aluminum tube.*

Using the published X-ray data, the team was able to accurately size a bone model to the residual limb and compare it with the X-ray. The stronger design incorporated two M10 bolts to withstand the 100kg load. An inner tube was included to allow wires to pass through.

The aluminum rod design was changed to an aluminum tube to facilitate wire passage and increase strength because of the larger diameter. The aluminum tube's diameter was 26.50mm, which is within the average range of femoral bone diameters [11], ensuring it was both realistic and robust.

### 3.2.4 Sensor Selection

After considering the issues with the preliminary sensors, the team decided to investigate other possibilities for sensors. The team selected a sonomicrometry system designed by Sonometrics Corporation (Sonometrics); this system utilizes piezoelectric crystals made of Lead Zirconate Titanate (PZT) to calculate distances between crystals. Prior to purchasing the device, an 8-channel system was rented to test whether it would work effectively in silicone with an aluminum metal core and sensors placed throughout the limb. It was also crucial to test whether this system would work in the presence of a strong magnetic field. This device is depicted in **Figure 18** below.



*Figure 18: 8-Channel sonomicrometry device that was rented from Sonometrics.*

Sonomicrometry is a technique for measuring the distance between piezoelectric crystals based on the speed of acoustic signals through the medium they are embedded in. Typically, the crystals are coated with an epoxy 'lens' and placed into the material facing each other. An electrical signal sent to one crystal is transformed into sound, which travels through the medium to the other

crystal. This second crystal converts the sound back into electricity, which is detected by a receiver. By calculating the time taken for the sound to travel between the crystals and knowing the speed of sound in the medium, the distance between the crystals is determinable [12].

To properly calculate the total tissue displacement around the limb, the team designed the following crystal placement. The guiding idea was to ground three of the 12 crystals on bony landmarks like the ischial tuberosity, greater trochanter, and distal femur to obtain a coordinate system for the remaining nine crystals. Using this method, the team obtained crystal data from nine distinct locations around the limb. **Figure 19** below shows the initial crystal placement concept for the 12-channel system.

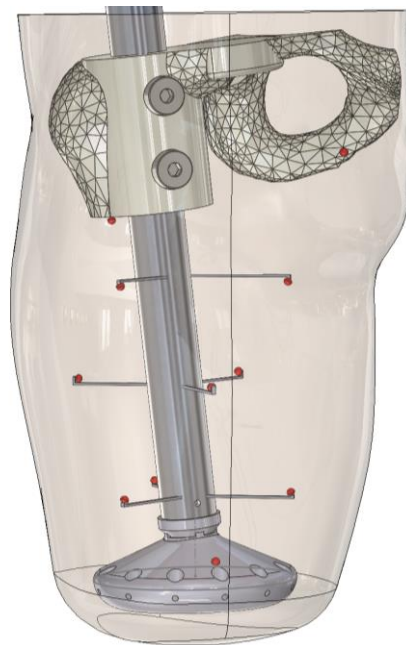


*Figure 19: Initial sensor placement concept for the sonomicrometry system. Red crystals represent the 2mm sonomicrometry crystals.*

To validate the sensor placement concept, the team constructed a half-scale model of this secondary design and implemented six sonomicrometry crystals into the model limb. These sonomicrometry crystals were the basic sensors available from Sonometrics, with no wire shielding or silastic

tubing around the sensors. **Figure 20** depicts the secondary half-scale model limb with the implanted sonomicrometry crystals. The cost of these crystals was \$85 per crystal.



*Figure 20: Secondary half-scale design with implanted sonomicrometry sensors.*

Upon testing the efficacy of the crystal placement and the sono crystal grounding method, the team realized the sensors had significant noise issues that could not be filtered out. To mitigate this, the limb was disassembled, and wire shielding was installed to test the sono system. With the new wire shielding, the system became significantly more reliable. This greater reliability, however, meant that the team now had to utilize the more expensive sensors from Sonometrics.

### 3.2.5 Mold Design

To improve the mold design based on the lessons gleaned from the preliminary one-piece mold, the group decided to design a more complex mold. For the second version, the mold was split into three parts with a part at the top to facilitate easier alignment of the bone. The team utilized 21 M6 x 75mm bolts to clamp the mold shut, ensuring that adequate pressure was applied to prevent the mold from breaking or opening during the molding process. **Figure 21** below depicts this secondary mold design.

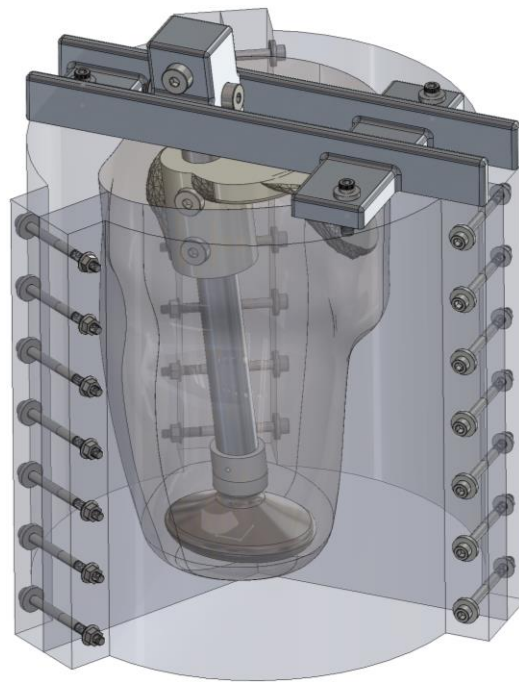


*Figure 21: Three-piece mold designed to ease bone placement and part removal.*

To evaluate the mold design, the group 3D-printed a half-scale version which allowed us to assess the surface quality of the final part and analyze the issues associated with using 3D-printed molds. During this process, the team also analyzed the sensor placement difficulty and accuracy to validate this mold design. **Figure 22** shows the 3D-printed mold in orange with the bone alignment tool 3D-printed in white.

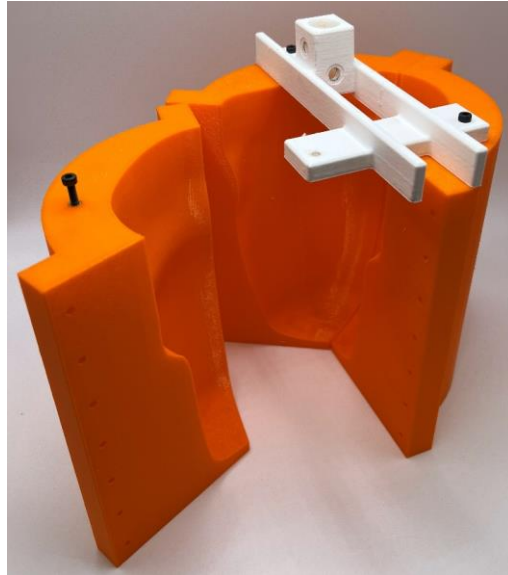


*Figure 22: 1/2 Scale 3D printed mold design (orange) with the bone alignment tool (white).*

To overcome the surface quality issues, the team considered using a combination of a 2-in-1 filler and sandable primer, a glazing spot putty, and sanding the 3D-printed part with 60, 80, 120, and 240 grit sandpaper to improve the mold surface quality. **Figure 23** represents a side-by-side comparison of these methods.



*Figure 23: Various methods of improving the mold surface quality. 2 in 1 sandable primer (left), glazing spot putty (middle), sanding (Right).*

Upon testing these methods, the team realized that sanding the mold reduced the layer lines but did not fully achieve the desired mold quality. To further improve the surface finish, we explored alternative methods for resurfacing the molds. The concept of utilizing a multi-piece mold design with additional alignment components was a pivotal step in the right direction.

Additionally, the team purchased a 15-gallon aluminum vacuum chamber from Best Value Vacs (BVV) with a V9D (9 cubic feet/minute) two-stage vacuum pump. This vacuum pump significantly improved the silicone quality and allowed for an improved degassing process. This vacuum pump can evacuate all air from the 15-gallon chamber within 5 minutes, achieving a vacuum pressure of -27 in Hg (-685.8 mmHg). The exact model and part number are listed in the appendix of this report.



### **3.2.6 Discussion: Secondary Design**

The secondary design of the model limb represented a significant improvement from the initial prototype. This iteration achieved a more anatomically correct shape, in large part because of the 3D scans obtained from the West Los Angeles VA Medical Center; these scans provided an accurate starting profile for the model limb, ensuring that the design closely mimicked a real transfemoral amputee's residual limb. The inclusion of X-ray validation for the model bone was crucial in this regard, allowing the team to size and orient the femur and pelvis accurately, thereby enhancing the anatomical fidelity of the model.

The adoption of a multi-part mold design was another critical advancement in the secondary design. This approach facilitated better alignment and easier demolding, addressing some of the significant challenges faced with the one-piece mold used in the initial design. By splitting the mold into three parts and incorporating additional alignment components, the team ensured that the final product could be assembled more precisely and removed without causing damage or deformation.

Even with these improvements, several issues continued to persist. One notable problem was that the model bone remained too bulky, which affected the overall aesthetic and potentially the functionality of the limb. Moreover, while using a multi-part mold design improved the process, the surface finish of the molded limb still exhibited imperfections. The layer lines from 3D-printing were not fully eliminated, even after extensive sanding and surface treatment efforts. This indicated the need for further refinement in mold preparation and finishing techniques.

Positioning sensors accurately within the model limb also proved to be a challenge. The complex geometry and the need for precise placement to ensure accurate measurements made this

task difficult. The initial sensors used in the secondary design were found to be inadequate, suffering from significant noise issues and lacking the necessary robustness. To address this, the team explored the use of higher quality sonomicrometry sensors, which, while more expensive, offered better performance and reliability.

In conclusion, the secondary design marked a substantial step forward in the development of a sensorized silicone model limb. The improvements in anatomical accuracy, facilitated by X-ray validation and a more precise mold design, were significant. However, issues related to the bulkiness of the model bone, surface finish quality, sensor positioning, and the need for better sensors highlighted areas for further development. Continued refinement and testing will be essential to overcome these challenges and achieve the desired level of performance and accuracy.

### 3.3 FINAL DESIGN

Using the concepts learned from the preliminary and secondary designs, the team finalized a feasible design while also adhering to the project design goals. It was crucial for this design to be anatomically accurate, represent a 100kg person, and be constructed and used with the existing infrastructure in the lab. **Figure 24** below shows simplified renderings of the design with and without the ferromagnetic implant side by side. The subsequent section will discuss the various design elements used to model the limb and explain justify why said elements resulted in an optimal design.



*Figure 24: Final Design renderings with (left) and without (right) the ferromagnetic implant.*

### 3.3.1 KUKA Attachment

After analyzing the various attachment methods discussed earlier in this report, the team decided to significantly alter the design to improve the anatomical resemblance while increasing the robustness of the design.

#### 3.3.1.1 KUKA Attachment Design

As the team worked through iterations, it became apparent that the M10 screw and bolt in the model bone had to be removed to reduce the bulkiness of the model bone. To overcome this issue while also ensuring that the bone was strong enough to withstand the 1000N loads present, the team decided to expand on the KUKA attachment design to include a supporting plate for the model bone. **Figure 25** below shows the final design of the KUKA attachment method.

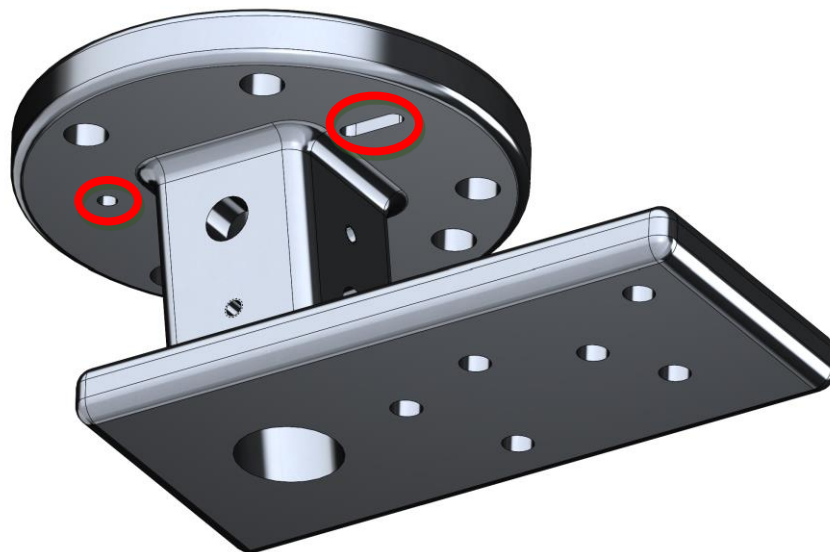


*Figure 25: KUKA Attachment method final design.*

Initially, to align this device to the KUKA mount presented earlier in this report (Figure 7), two M5 dowel pins must be inserted in the pin and slot on the top surface of the part. The alignment locations are represented by the red circles in **Figure 25** above. The pin is used to contain the part in two axes to prevent translation in x and y; however, the part can rotate about that pin. The slot

is used to constrain the part and prevent rotation about the pin. If the design had utilized two pins to align the structure, then the device would have been over-constrained, causing significant issues if the part were not machined properly. To mitigate this risk, the secondary pin was modified to a slot to accommodate any manufacturing issues.

To attach this device to the KUKA mount infrastructure, six M10 x 1.25 mm fine-thread alloy steel socket head screws that were 40 mm long with grade 5, zinc-plated steel washers were utilized. Finally, to ensure that the model bone was securely mounted to the KUKA attachment device, two 12mm alloy steel shoulder screws were used. Using shoulder screws allowed for loading the metal shoulder portion of the screw instead of the thread. To fasten these screws, two M10 x 1.5 mm high-strength steel nylon-insert locknuts were utilized. These nylon locknuts prevent loosening due to vibrations when the KUKA is moving through the gait profile. To overcome any alignment issues or slack due to manufacturing tolerances, the team also included four M5 x 0.8 mm stainless steel cup-point set screws to connect the bone more securely to the KUKA attachment.

### ***3.3.1.2 KUKA Attachment FEA Validation***

To analyze the strength of the newly designed KUKA attachment, SolidWorks Simulation was utilized. Through this application, we conducted a static motion study using the design-part geometry detailed in the previous section. We used Aluminum 6061 as the material for the study because of its strength and cost-effectiveness for machining a piece of this size. The device was fixed at the top of the surface, representative of its real-life application, as indicated by the green arrows in **Figure 26** below.

A 1000N load was applied to the edge of the attachment device to simulate a worst-case scenario, represented by the pink arrows in **Figure 26** below. A fine mesh was applied to the model to observe the strength of the design and analyze the effects of the screw holes around the part (depicted in **Figure 26**).

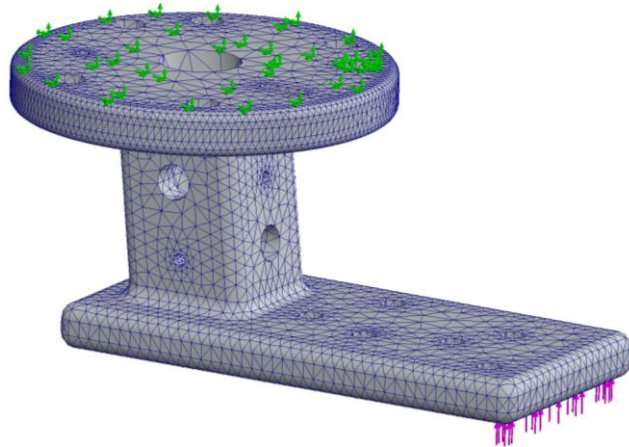


*Figure 26: Mesh design for the FEA analysis of the KUKA attachment device.*

Based on the results from the FEA, the yield strength of the part was determined to be  $5.515 \times 10^7$  N/m<sup>2</sup>. The peak stress experienced was  $5.224 \times 10^7$  N/m<sup>2</sup>, occurring at the red locations shown in **Figure 27** below. This stress level is below the yield strength of the part, indicating that the design can safely withstand the applied load without failure.

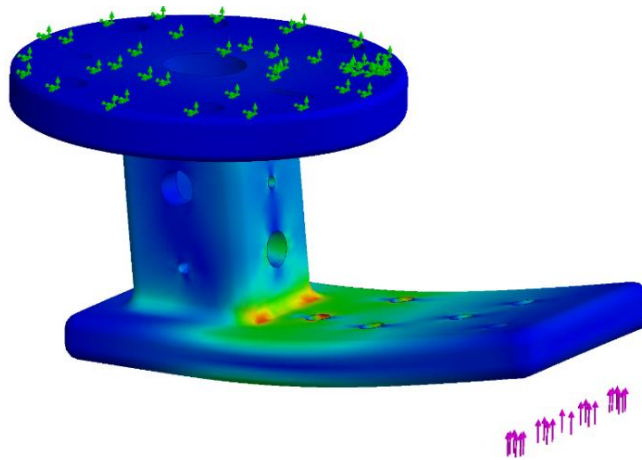


*Figure 27: Von Mises stress analysis. The peak stress was  $5.224 \times 10^7$  N/m<sup>2</sup>, and the yield strength was  $5.515 \times 10^7$  N/m<sup>2</sup>. The deformation is exaggerated for visual purposes.*

Under this applied load (1000N), the part experiences a maximum displacement of 0.4792 mm at the area shown in red in **Figure 28** below. This is not a major issue since the deformation amounts are less than half a millimeter.

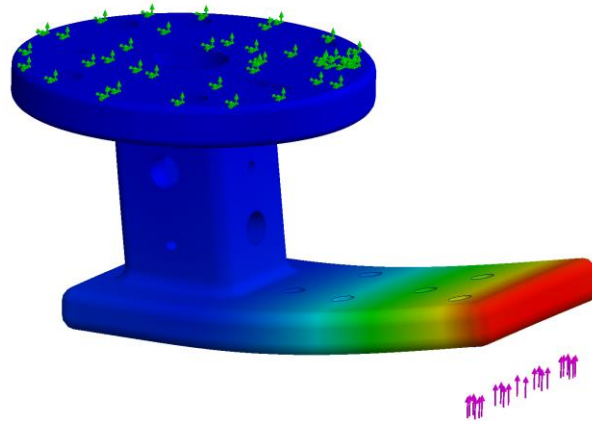


*Figure 28: Motion Study Displacement plot. The maximum displacement occurs towards the edge of the plate with a value of 0.4792 mm under the 1000N load. This figure is exaggerated for visual purposes.*

The maximum strain is in a similar area to the maximum stress (**Figure 29**), as expected. The maximum equivalent strain value was  $6.715 \times 10^{-4}$ , which is an acceptable value for this design.

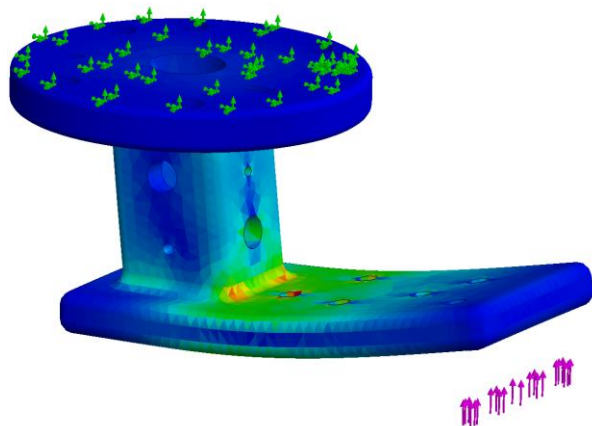


*Figure 29: Strain plot from the motion study. The maximum strain is  $6.715 \times 10^{-4}$  mm at the red locations. The figure is exaggerated for visual purposes*

Based on this FEA simulation, the team is confident that the KUKA attachment piece will withstand the present loads.

### 3.3.2 Limb Shape

After completing the construction of the secondary limb model, the team measured the tissue thickness around the implant and noticed an issue with the original shape of the limb. The minimum tissue thickness needed was 15 mm to prevent extrusion of the metal implants inside the limb. However, in two areas, the tissue thickness was only 12 mm; this discrepancy would cause the limb to inaccurately represent the conditions surgeons address during transfemoral amputations.

To overcome this issue, the model limb part file was modified to increase the bottom of the limb's diameter by 5 mm. This adjustment ensured the limb shape still matched the profile of some patients' residual limbs while providing the necessary tissue thickness. **Figure 30** below shows the modified limb profile design.

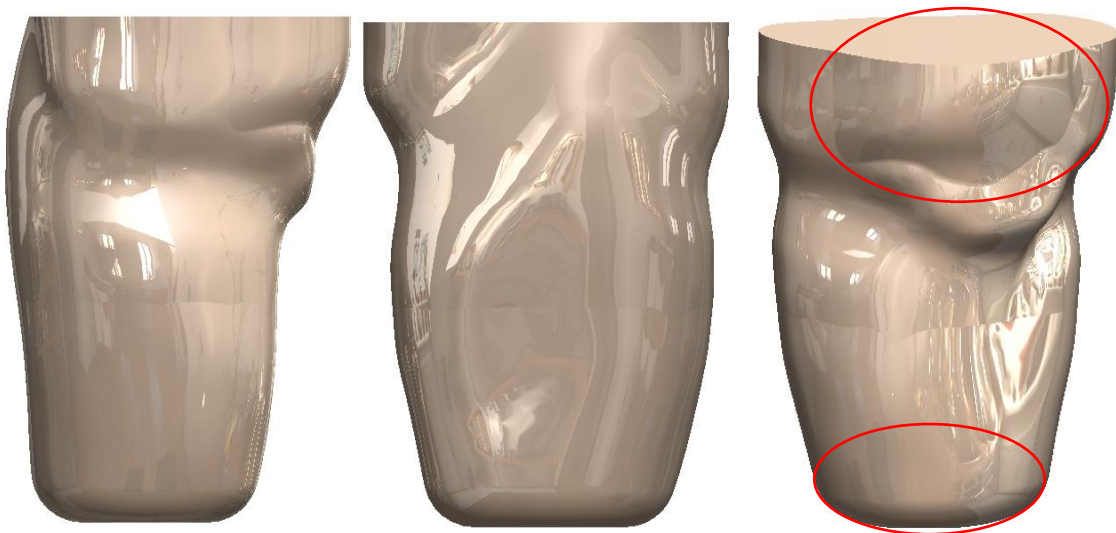


*Figure 30: Modified limb profile to better cover the pelvis and provide a minimum tissue thickness of 15 mm around the implant. Frontal view (Left), Side view (Middle), locations of the edit represented by the red circles (Right).*

Additionally, upon inspecting the pelvis, the team considered two options. The first option was to modify the pelvis bone to fit inside the limb, but this would weaken the pelvis because material would be removed from around the ischial tuberosity, which is load bearing. The second



option was to modify the top of the file and add additional tissue coverage around the pelvis. The team chose the second option to maintain the structural integrity of the pelvis.

The outer limb shape was edited to better contain the pelvis, and the bottom of the limb was adjusted to better contain the implant while preserving the overall integrity of the limb. The locations of these modifications are shown by the red circles in **Figure 30** above.

### 3.3.3 Bone Design

The goal of the final bone design was to implement improvements identified from the secondary bone design. The focus was on making the bone less bulky, better matching the anatomical shape, and enhancing the overall strength of the design. By refining the shape and structure based on detailed anatomical data and ensuring robust mechanical properties through advanced materials and FEA analysis, the team aimed to create a model that accurately represents a transfemoral amputee's residual limb while maintaining structural integrity under load conditions. This section details the design decisions, modifications, and validation processes undertaken to achieve the aforementioned objectives. **Figure 31** below depicts the final design of the bone model with (left) and without (right) the implant.



*Figure 31: Bone design for the case with an implant (left) and without an implant (right).*

### 3.3.3.1 Aluminum Tube

The bone design incorporates an aluminum tube for strength, which was sized based off published data regarding the average diameter of a femur. The selected aluminum tube had an outside diameter of 26.5 mm, compared to the average femoral bone diameter of 25.5 mm [11]. Using a part selected from McMaster, the team designed the connections needed to attach this model bone to the KUKA attachment device. We placed two 10mm through-holes, offset by 90 degrees at the top, to connect the aluminum tube to the KUKA attachment device.

Towards the distal end of the aluminum tube, we incorporated four 5 mm holes, also offset by 90 degrees. This was done to facilitate the implant attachment methods designed by another lab member. **Figure 32** below shows the final design of the aluminum tube.



*Figure 32: Aluminum tube design with various hole sizes and locations. The sensor wires will enter the tube from the slot location (green) and exit throughout the limb at the designated locations (red).*

Additionally, the team had to consider the locations for wiring holes. This was done by calculating the total wire diameter for each section of the limb and subsequently placing holes to

route the cables through. One 15 mm slot was placed at the top of the aluminum tube for sensor wires to enter and three 10 mm holes were placed around the aluminum tube for the sensors to exit at designated levels.

To finalize the location of these wiring holes, the team considered FEA results. Initially, the holes were placed on the same side of the tube to simplify machining, but this caused significant buckling under load due to the removal of material on the same side. After further analysis, the team finalized the hole locations.

To ensure accurate FEA results, a 1000 N load was applied at a 6-degree angle to match the model bone geometry, as indicated by the pink arrows in **Figure 33** below. We grounded the aluminum tube, shown by the green arrows, at the location of the M10 bolt holes. The maximum stress experienced was  $8.573 \times 10^6 \text{ N/m}^2$ , while the yield strength was  $5.515 \times 10^7 \text{ N/m}^2$ .

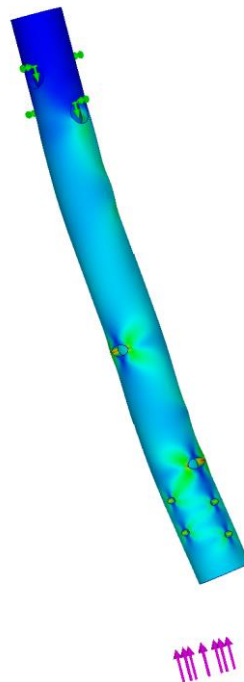


*Figure 33: SolidWorks Simulation von Mises stress plot. The maximum stress was  $8.573 \times 10^6 \text{ N/m}^2$ , and the yield strength was  $5.515 \times 10^7 \text{ N/m}^2$ . The peak stress is experienced at the holes designed for wiring towards the bottom of the limb. The figure is exaggerated for visual purposes.*

The maximum displacement was 0.02133 mm at the distal end of the bone. This is a trivial amount of deformation and is acceptable for our model limb. **Figure 34** below shows the maximum deformation location for this bone model in red.

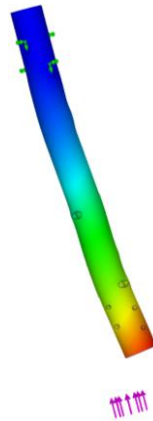


*Figure 34: SolidWorks displacement plot. The maximum displacement at the distal end of the bone was 0.02133 mm. This figure is exaggerated for visual purposes.*

The maximum strain was  $8.881 \times 10^{-5}$ , shown in the red regions in **Figure 35** below. This deformation occurs at the M10 hole locations used to route the wires through the limb.

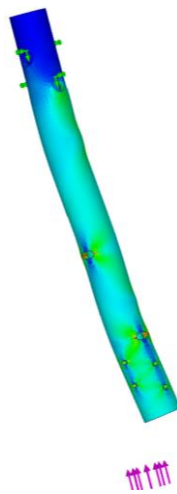


*Figure 35: The SolidWorks strain plot. The location of the maximum strain is similar to the location of the maximum stress, which is near the holes designed for the wiring. This figure is exaggerated for visual purposes.*

The values obtained from this simulation validate the aluminum tube design. The team is confident that this design will be able to withstand the applied loads.

### 3.3.3.2 Bone Cover Final Design

As mentioned in the secondary bone design section (section 3.2.3), the final design of the bone cover was derived from an STL file of a cadaveric femur pelvis bone scanned using a 3D scanner. By using X-ray data, the STL file was sized to match the model limb's dimensions. To facilitate the implant attachment method, we placed holes towards the bottom of the model bone. Additionally, to ensure that the sono crystals could be grounded properly, the team utilized three standoffs, enabling the connection and grounding of the crystals. To prevent the sono wires from interfering with the line of sight of the crystals, we cut three grooves into the bone cover, allowing the cables to be routed through the 3D-printed part. **Figure 36** below depicts the bone cover design with the location of the sono standoffs circled in red.

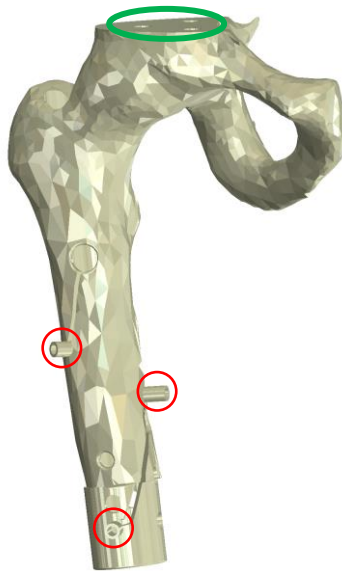


*Figure 36: Finalized model bone cover design. The location of the three standoffs used to ground the sono crystals is shown by the red circles. The location of the threaded inserts is represented by the green circle.*

To connect this model bone to the KUKA attachment plate, three 12mm long M6 threaded inserts were installed at the top of the bone cover above the pelvis (depicted by the green circle in

**Figure 36** above). Using three M6 bolts and washers, the team attached this part to the KUKA attachment device.

To validate the structural integrity of the bone cover, we performed FEA using SolidWorks Simulation applying a 1000N force to the ischial tuberosity (pink arrows depicted below), which serves as the hard stop for ischial containment sockets. As depicted in **Figure 37**, we selected a fine mesh setting, and the green arrows represent the grounding locations for the bone cover.

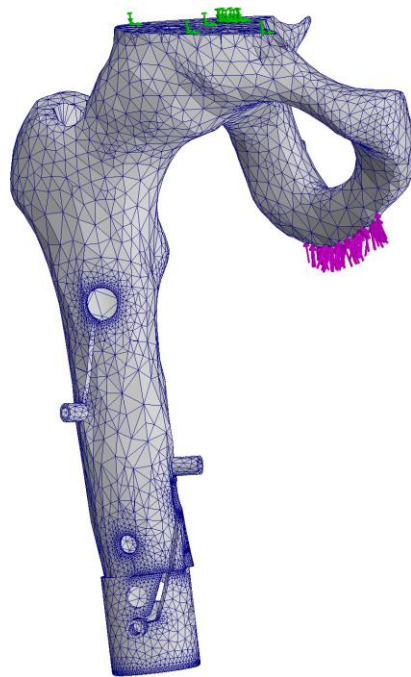


**Figure 37:** Model bone mesh design. The force is applied on the ischial tuberosity, which is the hard stop used for ischial containment sockets. The green arrows represent the grounding location.

We selected Markforged Onyx filament as the material for this simulation. Onyx is a micro carbon-filled nylon designed exclusively for Markforged 3D printers. To input the material properties into SolidWorks, the team used the Onyx datasheet values, such as its tensile modulus (2.4 GPa) and yield stress (40 MPa), to simulate the material [13]. We obtained the following results using a static trial with the conditions listed above.

Based on the FEA results, the maximum stress experienced by the ischial tuberosity part of the pelvis was  $1.796 \times 10^8 \text{ N/m}^2$  (**Figure 38**). The maximum strain value was  $8.047 \times 10^{-2}$  and occurred at the same location as the maximum stress.



**Figure 38:** SolidWorks simulation stress plots. The maximum stress is experienced at the ischial tuberosity with a value of  $1.796 \times 10^8 \text{ N/m}^2$ . The maximum strain value was  $8.047 \times 10^{-2}$ . This figure is exaggerated for visual purposes.

The maximum displacement occurred above the ischial tuberosity with a value of 2.923 mm for the full 1000 N load. The displacement is indicated by the red zone in **Figure 39** below.



**Figure 39:** SolidWorks simulation deformation plots. The maximum displacement is experienced at the ischial tuberosity with a value of 2.923 mm.



Based on the values obtained from the FEA simulation, we are confident that this design will be able to withstand the applied loads while maintaining anatomical accuracy and structural integrity. The bone cover achieved its design target of better matching X-ray data and reducing bulkiness. The FEA analysis—which used Onyx material—demonstrated that the design could withstand the forces experienced.

### ***3.3.3.3 Distal Femur Bone Model***

For the no-implant case, the team aimed to mimic the bone size and tissue gap to the outer surface of the limb; this was achieved by reviewing published data on the average size of the femoral canal and the gap distance between the end of the distal femur and the surface of the skin. The mean diameter of the femoral canal for males was found to be 13.3 mm [14]; therefore, we selected an inner diameter of 13.5 mm for the model bone. Based on this data, the following design—depicted in **Figure 40** below—was created to act as a distal bone model.

Additionally, it was crucial that this design allowed the team to place pressure sensors around the distal end of the bone. Therefore, the bottom of the design was modified to enable the pressure sensors to be securely fixed to the model bone.

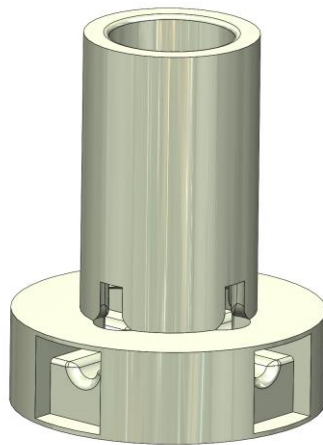


*Figure 40: Distal femur bone model for the no implant case.*

### 3.3.4 Sensor Selection

The importance of choosing sensors was twofold. First it was crucial that the sensors were able to detect pressure at key locations such as the distal femur, the ischial tuberosity, and the greater trochanter. Second, the team needed sensors to detect local tissue deformation which is defined by the tissue movement at various locations around the model limb relative to the bone. To complete this task, we identified sonomicrometry as the the most optimal method of measuring local tissue deformation. Another team member was able to identify a pressure sensor that was also capable of detecting the temperature at that location. This section of the report will discuss the sensor selection process and explain the overall design which can be seen in the figure below.



*Figure 41: Final limb model with implemented sensors and wiring with(left) and without (right) the implant.*

### 3.3.4.1 Sonomicrometry

As previously explained, sonomicrometry is a technique used to measure the distance between piezoelectric crystals by analyzing the speed of acoustic signals through the medium in which they are embedded. Typically, these crystals are coated with an epoxy 'lens' and placed facing each other within the material. An electrical signal sent to one crystal is converted into sound, which travels through the medium to the other crystal. This second crystal converts the sound back into electricity, detected by a receiver. By calculating the time taken for the sound to travel between the crystals and knowing the speed of sound in the medium, the distance between the crystals can be accurately determined [12]. **Figure 42** below shows the sonomicrometer system purchased from SonoMetrics Corporation.



*Figure 42: Digital 12-channel transceiver sonomicrometer hardware from SonoMetrics Corporation. An additional 12-channel breakout box is used to extend the sensors wire lengths. The device costs \$16,000, and the breakout box costs \$700.*

The team selected the 12-channel system and purchased 12 sonomicrometry crystals on one meter of silastic wiring, each costing \$106.25. These sensors are designed to be kept in the model limbs, which requires a total of 48 sonomicrometry crystals for the entire project. Subsequent sections will detail the crystal grounding method, the positioning, and the device's integration with the existing infrastructure.

#### 3.3.4.1.1 Grounded Crystal Design and Position

To ensure the accuracy of the soft tissue movement data obtained from the 12-channel system, three of the crystals had to be grounded; these grounded crystals allow the team to create a coordinate frame, allowing for the movement calculation of the remaining crystals with respect to that frame. The purple circles in the figure below represent the grounded crystals 1,2, and 3.

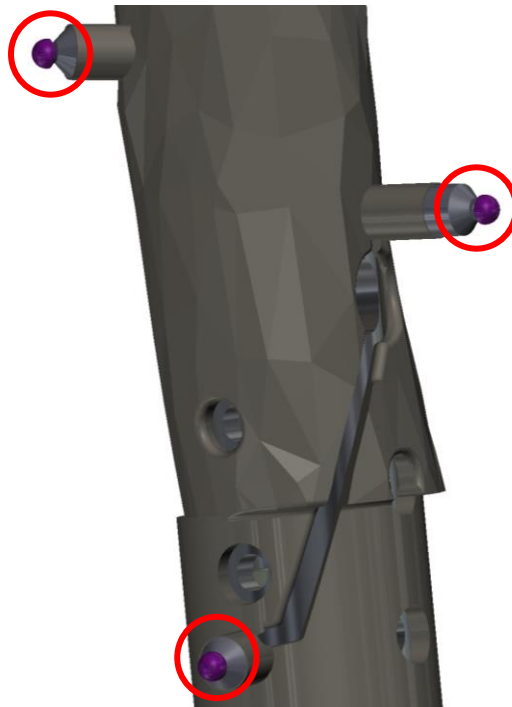


*Figure 43: Close-up view of the grounded crystal design and position. Crystal 1 is the purple crystal on the right, crystal 2 is towards the bottom, and crystal 3 is on the top left of the figure.*

To secure the grounded crystals to the bone without damaging their wires, I designed special standoff inserts with two key concepts in mind. First, the standoffs needed to avoid blocking the line of sight of the crystals; this was achieved by incorporating a chamfer design at the edge. Second, the standoffs had to be securely attached to prevent any movement of the crystals; this design successfully grounded the first three crystals, establishing a reliable coordinate frame for accurate movement measurement.

#### 3.3.4.1.2 Sonomicrometry Crystal Placement

To accurately calculate the silicone movement data throughout the limb, the team determined that the remaining nine sono crystals must be strategically distributed. Initial tests revealed that the maximum reliable distance between crystals in silicone should not exceed 15 cm. Distances greater than 15 cm result in inaccurate data measurements. Further analysis using the triangulation method for positioning these crystals concluded that each crystal must be visible to at least three other crystals to ensure precise data collection.

It is essential to note that sono crystals can detect other crystals in all directions except in the direction of the crystal's wire. Consequently, the orientation of the crystals was crucial for the success of the device. With these considerations in mind, the team methodically placed the crystals, one at a time. To achieve effective triangulation of both the front and back sides of the limb, the crystals were organized into three groups of three. Each group was positioned on a different level along the limb: the bottom level approximately 4.5 centimeters from the limb's base, the middle level about 12.5 centimeters up, and the top level around 20 centimeters from the base.

Within each level, the crystals were spaced 120 degrees apart to facilitate communication among them. The crystals on the middle level were additionally rotated by 60 degrees to enhance connectivity between the crystals on the bottom level and those at the very top. **Figure 44** below illustrates the final placement of the crystals, displaying the strategic arrangement designed to maximize data accuracy and sensor functionality.

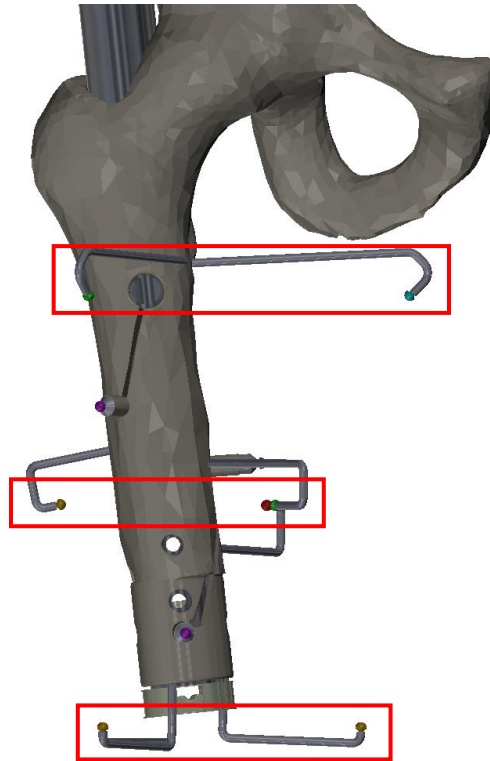


***Figure 44:** Finalized crystal placement, demonstrating the strategic distribution and orientation of sono crystals on different levels of the limb for optimal data triangulation. The top box consists of crystals 5, 9, 11. The middle box consists of crystals 4, 6, 12. The bottom box consists of crystals 7, 8, 10.*

The placement and orientation of the sono crystals are meticulously designed to optimize data accuracy while minimizing potential interference. The crystals in the middle level are intentionally pointed inwards to enhance their communication capabilities with the neighboring crystals. However, this inward orientation poses a challenge as the wires connected to these crystals may block the line of sight of others, which is crucial for accurate sonomicrometry.

Therefore, careful consideration was given to the routing and placement of the wires to avoid any potential disruption in crystal communication.

Additionally, to ensure accurate deformation measurement near the bone, the crystals in the middle level are positioned closer to the bone compared to those at the top and bottom levels of the limb; this strategic placement improves the effectiveness of the data collected regarding bone movement and strain and helps maintain a clear line of sight for the sonomicrometry measurements across various parts of the limb.

The degree of precision in the placement of crystals and their wires is vital for achieving reliable and meaningful data from sonomicrometry, especially in a complex medium like silicone where sound transmission can be easily obstructed. The team's efforts to optimize crystal positions and address potential obstructions reflect a robust approach to ensuring the system's overall functionality and effectiveness in biomechanical assessments.

#### 3.3.4.1.3 Breakout Box Attachment Design

Given the sensitivity of the sonomicrometry device to movement and its considerable cost, the team opted to keep the sonomicrometer stationary on a table while allowing the sensor extension, known as the breakout box, to move with the simulated limb motion. Recognizing that the crystal wires were only 1 meter long and the KUKA robot would simulate walking movements, the team selected a breakout box equipped with a 4.88-meter (16 ft) extension cable. The intention was to mount the breakout box on the KUKA robot, while the sonomicrometer itself would be placed in a secure, stationary location.

To facilitate this, the team designed a specific attachment part for mounting the Sonometrics breakout box (see **Figure 42**) to the KUKA robot; this design is depicted in **Figure**

45 below. The breakout box is mounted to this custom-designed part using nuts and bolts, ensuring a sturdy and reliable connection.

To secure this attachment to the actual KUKA, the piece was designed for a press-fit onto the end effector of the KUKA. However, to ensure additional stability, especially given the dynamic movement of the KUKA during simulations, the team incorporated two Velcro straps to prevent any displacement. After printing and testing this design, the team believes the attachment is both adequate and secure for its intended use, providing a stable platform for the breakout box during active limb simulations.

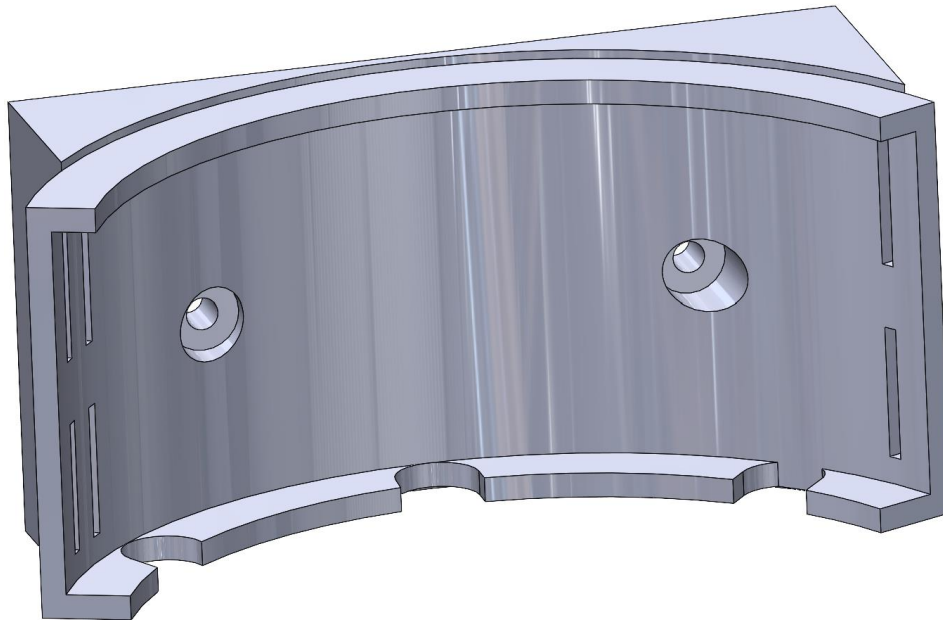


*Figure 45: Sonomicrometer breakout box KUKA attachment. The breakout box is fastened to this piece using screws and bolts. Once fastened, this part secures to the KUKA with Velcro straps.*

This attachment solution addresses the operational challenges of integrating sensitive electronic equipment with dynamic robotic movements, ensuring both the functionality and safety of the sonomicrometry setup.



### 3.3.4.2 Pressure & Temperature Sensors

To complement the sonomicrometry system, the team integrated pressure and temperature sensors into the limb model to enhance the collection of biomechanical data. These sensors are strategically placed at key anatomical landmarks and areas of interest within the limb (**Figure 46**); doing so provides detailed insights into the internal pressures and temperature variations during movement simulations [15] [16]. These locations were selected based on published data. [17]

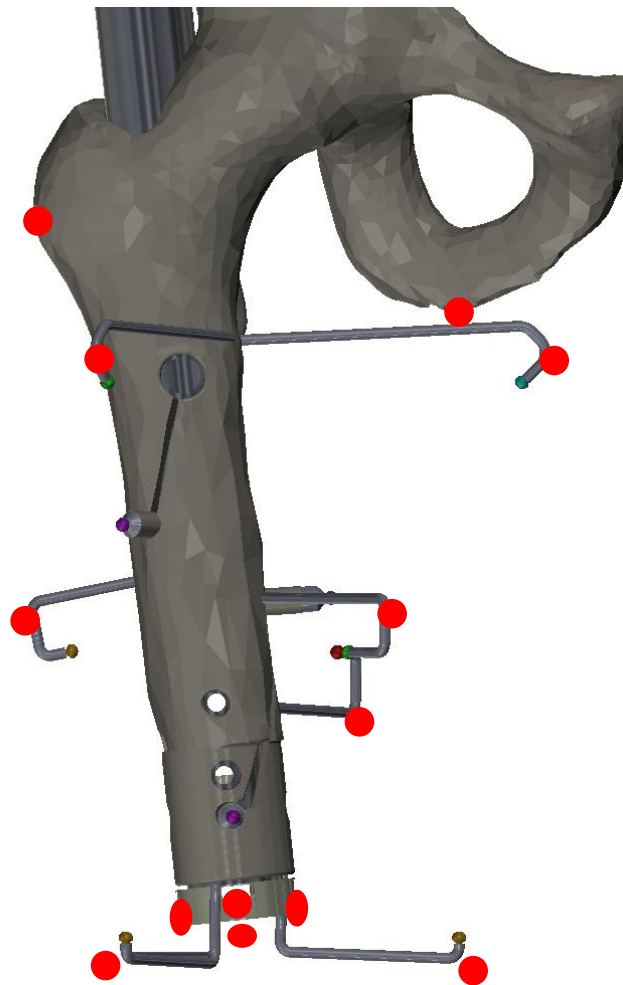


*Figure 46: The 16 pressure sensors' locations relative to the sono crystal placement. Three of the pressure sensors are on the back side of the limb and are not visible.*

The placement of the 16 pressure sensors was measured meticulously to maximize the utility of the data collected. Sensor 1 is located at the ischial tuberosity, a critical point for pressure

monitoring due to its load-bearing capacity. [17] Sensor 2 is positioned at the greater trochanter, an area that experiences significant pressure during the limb's lateral movements and when lying on the side. Sensor 3 is situated at the distal femur, providing data on pressures exerted at the lower end of the thigh bone, which is crucial for prosthetic fittings [15].

Sensors 4 through 12 are co-located with their respective sono crystals to ensure that the pressure data can be correlated directly with the spatial movements detected by the sonomicrometry system; this integration allows for a comprehensive analysis of how internal pressures relate to changes in the limb's geometry during simulated activities.

Sensors 13 through 16 are placed around the distal femur bone model, as described in section 3.3.3.3. These sensors aim to capture pressure data from all locations towards the bottom of the bone, providing critical comparisons between cases with and without the ferromagnetic implant; this approach helps validate the limb model's design and offers essential insights into the potential impacts of prosthetic choices on the limb's biomechanics.

By capturing pressure and temperature data at these specific locations, the team can analyze the distribution and variation of internal forces and temperature within the limb under different conditions. This analysis is invaluable for refining prosthetic designs and improving the comfort and functionality of limb prostheses for amputees.

#### ***3.3.4.3 Wire Grommet Design***

To safeguard the integrity of the sensor wires and prevent potential damage during operation, designing effective wire grommets became a critical consideration in the construction of the limb model. The primary goal was to ensure that the aluminum structure of the limb did not

cut into or abrade the cables with use, which could lead to wire failure and inaccurate data transmission.

Initially, the team opted for standard rubber grommets designed for wire protection. However, it became apparent that the rubber material interfered with the silicone curing process, rendering them unsuitable for use within the limb model. The team then explored the option of silicone grommets, which would not inhibit the curing process. Unfortunately, these were not compatible with the contours of the pipes, because they failed to provide a snug and secure fit.

Faced with these challenges, we decided to customize grommets that could meet all the specific requirements. These grommets were tailored to fit the exact hole size and match the curvature of the aluminum pipes precisely. To achieve this, the team opted to design, and 3D print the grommets using a PLA which is compatible with both the silicone limb and the embedded sensor wires. **Figure 47** below shows the 3D grommet design.

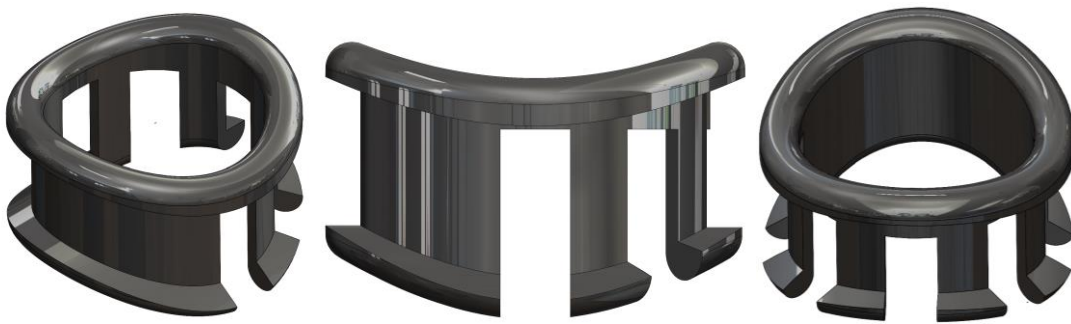


*Figure 47: 3D grommet design which prevents damage to the cables.*

This customized approach allowed for a perfect fit that protected the wires effectively without compromising the functionality of the limb or the curing process of the silicone. The bespoke grommets ensured that the wires were adequately shielded from any sharp edges or abrasive surfaces within the aluminum structure, thus maintaining the longevity and reliability of the sensor system.

### 3.3.5 Mold Design

Building on the improvements and lessons from the secondary mold design, the team developed a final mold design to optimize the manufacturing process and enhance the quality of the silicone limb models. This final design incorporated feedback and testing results from previous iterations, ensuring robustness, precision, and ease of use.

To further improve sensor positioning, mold construction, and part removal, the team designed a six-part mold, replacing the previous three-part design. This multi-part mold allowed for more precise alignment and easier management during the molding process. **Figure 48** below shows the final mold design that will help construct the model limbs.

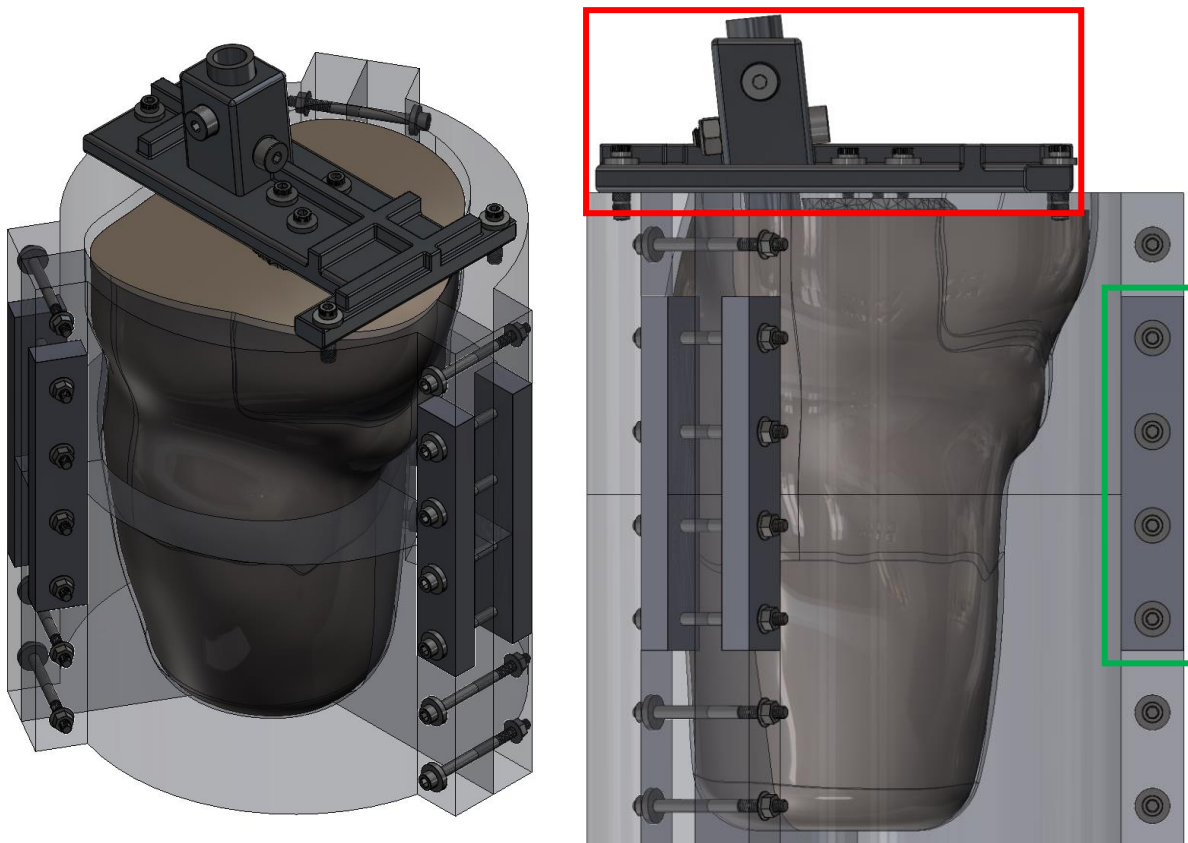


*Figure 48: Isometric (left) and side view (right) of the final mold design. The top piece surrounded by the red box is the limb alignment device used to position the model bone within the limb. The piece surrounded by the green box is used to connect the top and bottom halves of the mold.*

Similarly to the secondary mold design, the mold is clamped using 21, 75mm M6 bolts. However, with this design, one mold piece can be taken apart while the remaining five pieces remain intact. This feature is crucial for sensor positioning and bone alignment. The parts were designed to fit within the 3D printer's build volume and the 15-gallon vacuum chamber for 3D printing these molds.

### **3.3.6 Discussion: Final Design**

The final design of the silicone model limb represents the culmination of extensive research, iterative improvements, and rigorous validation. Throughout the project, major design concerns were meticulously addressed, resulting in a robust and reliable limb model that meets the project's stringent requirements.

One of the primary concerns was ensuring the anatomical accuracy of the limb model. The bone and soft tissue structures were carefully modeled based on anatomical data and validated through X-ray comparisons to accurately represent a 100kg person with a transfemoral amputation; this degree of precision was crucial for the model's functionality and realism.

The integration and placement of sonomicrometry crystals and pressure sensors were optimized to provide precise biomechanical data. The six-part mold design facilitated the accurate positioning of sensors and proper alignment of the bone, enhancing the overall effectiveness of the limb model; this modular approach allowed for efficient assembly and disassembly, which was necessary for sensor placement and part removal.

Ensuring material compatibility was another critical factor in the design process. The selection of materials, such as aluminum for structural components and onyx filament for the bone cover, guaranteed the model's durability and performance. Bespoke grommets protected the sensor wires without interfering with the silicone curing process, addressing the issue of material incompatibility encountered with off-the-shelf grommets.

Finite Element Analysis played a pivotal role in validating the strength and durability of the model components. By simulating double the expected loads, the team ensured that each part could withstand extreme conditions without failure. The FEA results provided confidence in the

structural integrity of the design, confirming that the limb model could endure the stresses of simulated walking and other dynamic activities.

While each component of the limb model was designed separately to address specific needs, they were meticulously integrated to function as a cohesive system. The careful alignment and integration of components ensured that the model maintained its anatomical accuracy and mechanical stability.

The final design of the silicone limb model successfully addressed all major design concerns. The use of FEA for validation, the modular approach to the component design, and the integration of advanced sensor systems culminated in a high-quality and reliable model. This model not only meets the project's goals but also provides a valuable tool for further biomechanical research seeking to develop improved prosthetic solutions.

The iterative design process, informed by rigorous testing and validation, has resulted in a limb model that is both anatomically accurate and mechanically robust. The final product is well-suited for detailed biomechanical studies and sensor integration, marking a significant advancement in prosthetic limb research.

## 4 CONSTRUCTION

---

The construction phase of the silicone limb model involved several key steps, each precisely executed to guarantee the final product's accuracy, durability, and functionality. This section outlines the processes and methodologies employed in building the model, from initial preparations to final assembly.

### 4.1 KUKA ATTACHMENT CONSTRUCTION

After validating the part through a design review and receiving approval from my advisor, the team 3D printed a prototype to mount on the KUKA robot for initial testing. After reviewing the alignment and part geometry, the part was finalized. The part's finalized object file along with its detailed drawings, was sent to SuNPe in China for manufacturing (**Figure 49**). The engineering drawing and prototyping quote is attached in the Appendix section of this report. The total cost for this part was \$500.



*Figure 49: The machined KUKA attachment.*



## 4.2 MODEL BONE CONSTRUCTION

The construction of the model bone involved two key steps. First, the model femur and pelvis had to be 3D printed and finalized. Second, the aluminum tube had to be machined and prepared for assembly. **Figure 50** below shows the finalized construction of the model bone for the case with the ferromagnetic implant.



*Figure 50: Model bone construction for the case with the ferromagnetic implant.*

#### 4.2.1 Bone Cover Construction

Initially, the team printed the model bone using PLA; however, upon stress testing, the material fractured. As a result, the team 3D printed the model bone using the Markforged 2 printer with onyx material. The print was designed with a 45% infill density and a 2mm wall thickness to ensure adequate strength. **Figure 51** below depicts the printed pelvis on the Markforged Mark 2 print bed. Due to build volume limitations, the team printed the femur separately to ensure that the parts would fit within the print volume. The total print time was 26 hours and 15 minutes.

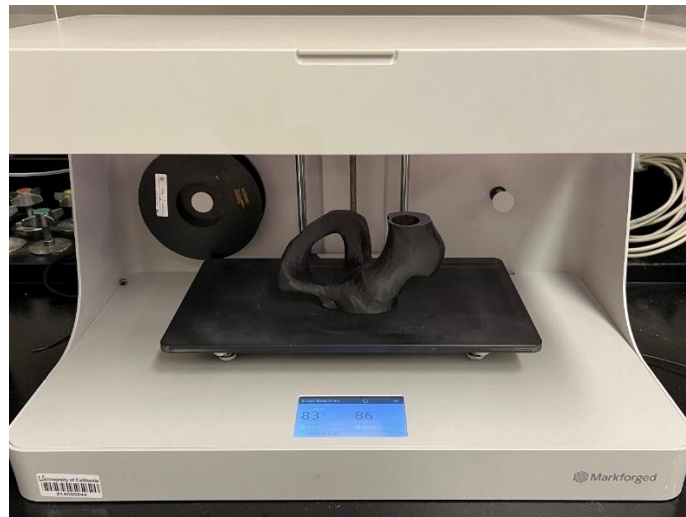


*Figure 51: Markforged Mark 2, 3D printer with the pelvis printed with Onyx.*

To attach the parts together, various adhesives were tested, such as Gorilla Super Glue and Loctite 1364076 Super Glue; these adhesives inhibited the curing of silicone due to their sulfur content. Ultimately, 3M Scotch-Weld Plastic & Rubber Instant Adhesive PR40 was used to glue the printed parts together effectively. After the parts were printed and glued together, heat inserts were installed. The KUKA robot was then used to apply measured forces, affirming the strength of the printed bone.

## 4.2.2 Aluminum Tube Construction

To machine the aluminum tube, six feet of aluminum tubing with the correct diameter was ordered from McMaster-Carr. First, the tube was cut to the appropriate size using a band saw. The tube was placed in a rotary chuck on a milling machine to begin the machining process. Using an end mill, one side of the pipe was faced off to ensure that the pipe had a good working edge. Using that side and the engineering drawings provided in the Appendix, the holes were drilled according to the specified sizes and locations; this machining took place at the UCLA machine shop. **Figure 52** below depicts the components required to assemble the bone model.

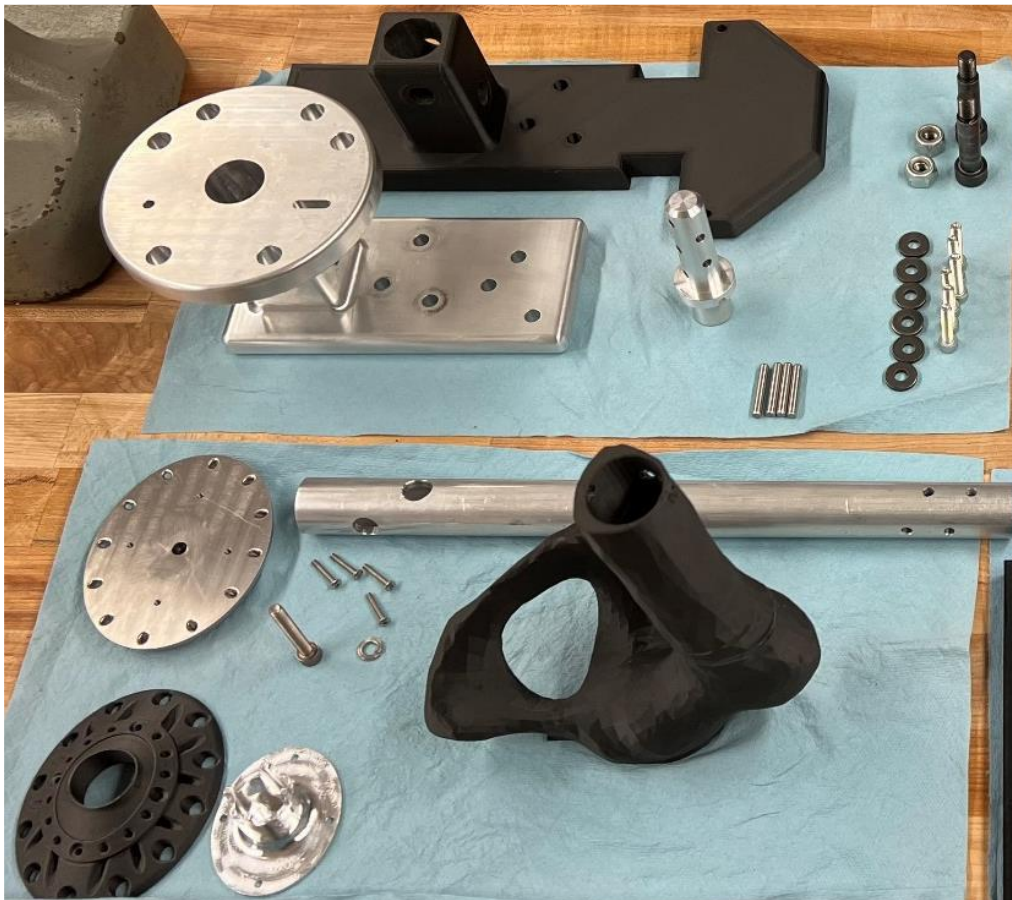


*Figure 52: Machined aluminum tube with the various components and fasteners needed to assemble the bone model for the case with the implant.*

### 4.3 SENSOR CONSTRUCTION

The pressure sensors utilized in this project were designed by another team member and constructed at the UCLA Maker Space. The construction process involved several detailed steps to ensure the precision and reliability of the sensors. To begin the construction of the pressure sensors, a tin stencil was used to apply solder paste accurately to the printed circuit board (PCB). The stencil ensures that the paste is applied precisely to the pads where the components will be mounted; this step is crucial for achieving reliable electrical connections and proper component placement. After the solder paste was applied using the stencil, the PCBs were prepared for component placement (see **Figure 53** below).

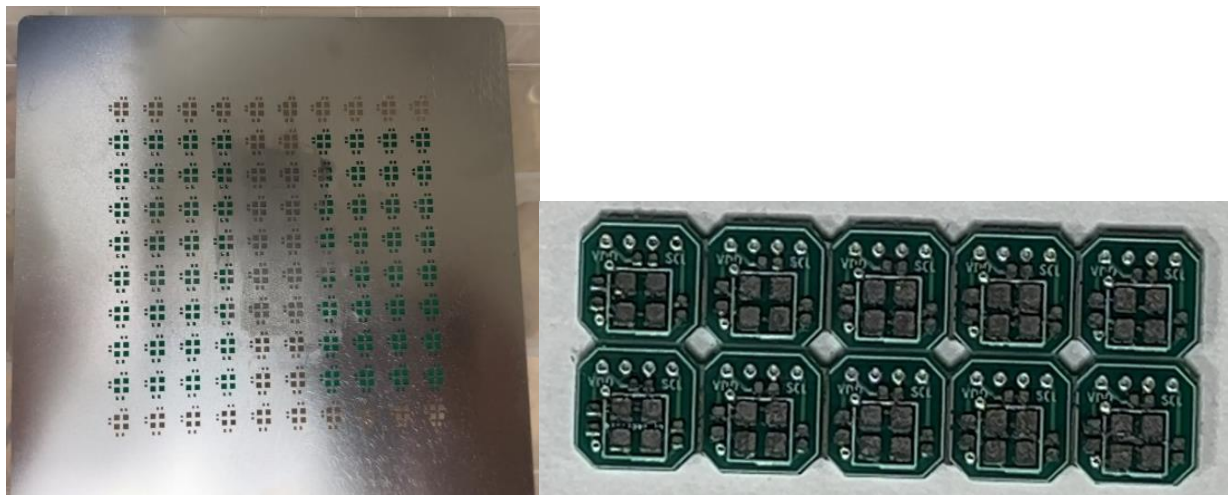


*Figure 53: The tin stencil used to apply solder paste to the PCB prior to installing the components (left). The PCB board for 10 pressure sensors with the applied solder paste (right).*

The next step consisted of placing the components onto the PCB. Each pressure sensor board required the placement of two resistors, one capacitor, and one pressure sensor. These components were carefully positioned on the PCB, to ensure that they aligned correctly with the pads coated in solder paste; this is illustrated in **Figure 54** below. Proper placement is essential for the functionality of the sensors and the integrity of the solder joints formed during reflow soldering.



*Figure 54: The 10 completed pressure sensors with two resistors, one capacitor, and one pressure sensor that were installed prior to being placed in the oven for the solder's melting.*

Once all components were placed on the PCB, the boards were placed in a reflow oven. The oven was heated to 170°C, which is the melting point of the solder paste. The heat causes the solder paste to melt, creating strong and reliable solder joints between the components and the PCB. This reflow process ensures that all connections are securely made and that the components are attached to the board. Monitoring the temperature and time in the oven is critical to avoid overheating, which could damage the components. **Figure 55** depicts the reflow oven used and what the sensors looked like after heating.

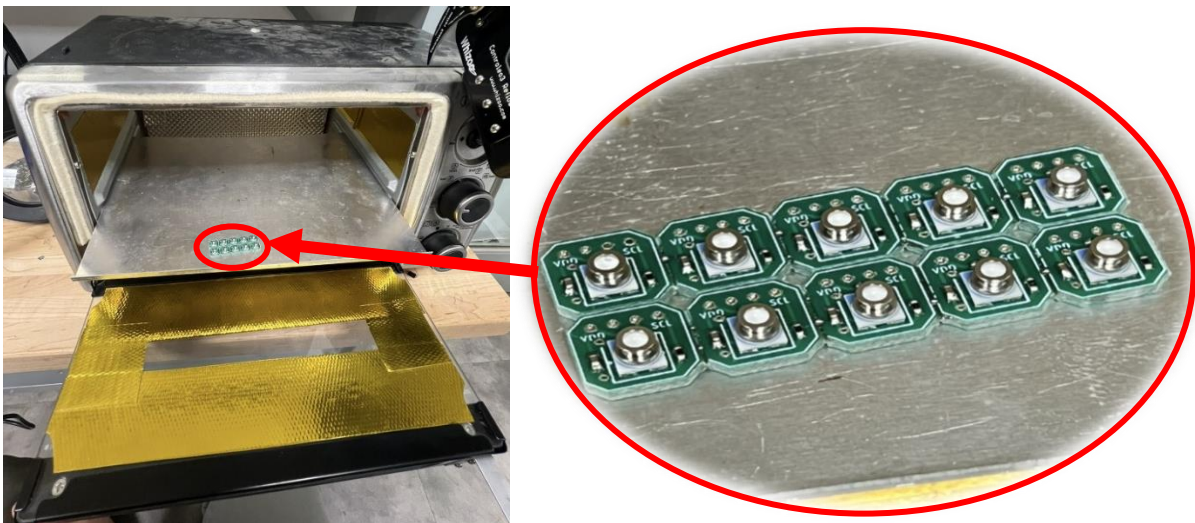


*Figure 55: The reflow used to heat the solder paste to 170°C.*

After the soldering process was complete, the finalized pressure sensors were equipped with shielded wiring (**Figure 56**). Shielded wires are used to protect the signal integrity of the sensors, minimizing electromagnetic interference, and ensuring accurate readings. The shielded

wiring is crucial for maintaining the performance of the sensors in environments where electronic noise can affect the measurements.



*Figure 56: The 16 finalized pressure sensors with the shielded wiring installed.*

Constructing the pressure sensors through this meticulous process ensured that each sensor was reliable and functional. The combination of precisely applying the solder paste, accurately placing the components, and controlling reflow soldering resulted in high-quality sensors ready for integration into the silicone limb model.

By following the aforementioned steps, the team successfully produced a set of robust pressure sensors capable of delivering accurate data for biomechanical research and prosthetic development. The attention to detail in the sensor construction process highlights the importance of precision and care in producing devices that yield reliable data.

## 4.4 MOLD CONSTRUCTION

### 4.4.1 3D Printing (-10% Volume, Nominal, +10% Volume)

Based on the mold design requirements, it was crucial that the limb volume could change. The team aimed to understand the effects of limb volume on prosthetic socket fitment. To address this, the molds were printed with three different limb volumes: -10%, nominal, and +10%.

The mold construction process involved extensive 3D printing, amounting to 432 hours to print all 18 parts. The molds were printed using Eco ABS Filament on a Dremel 3D45 printer (see **Figure 57** below), with a 5% infill and a 2mm wall thickness. Each of the six parts took approximately 24 hours to print, requiring about 125 meters of filament per part. To ensure successful printing, the process was monitored every 8 hours to check for print failures.

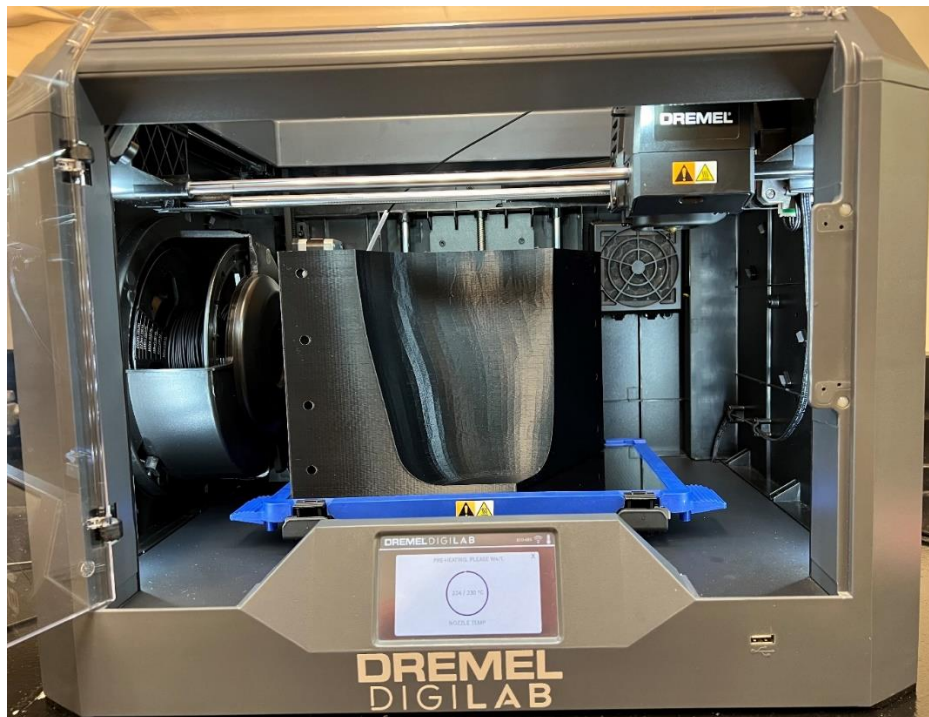


*Figure 57: The Dremel 3D45 used to print the mold and bone alignment parts.*

To ensure that the bone alignment part (see **Figure 58** below) would not bend due to the weight of the model bone, the team incorporated I-beam-like structures on the top surface of the

part. These beams add additional material above the part, significantly strengthening the part and preventing it from bending. Furthermore, the bone alignment part was printed with a 50% infill to ensure it could withstand the weight of the model bone.

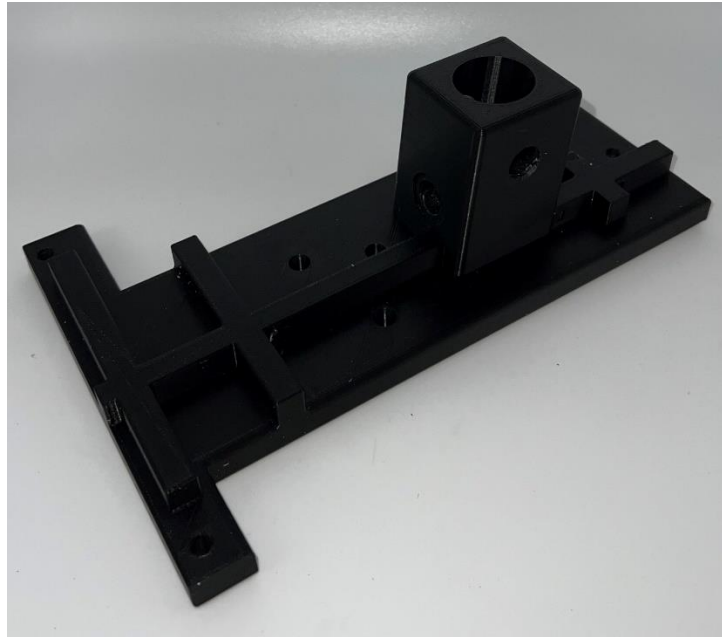


*Figure 58: The Bone alignment part that was printed using Eco ABS filament on the Dremel 3D45.*

To achieve a high-quality surface finish, the molds were sanded with 60, 120, and 240 grit sandpaper using a Dremel rotary tool. The edges of the parts were subsequently covered using masking tape and XTC-3D was applied to fill in the layer lines and create a glass-like shiny finish. To ensure a good surface quality, the XTC-3D was applied in two coats. The first coat consisted of a thin layer to provide even coverage without any air bubbles. Once the first coat had cured, a second thicker coat was applied to the XTC-3D. This step significantly improved the surface quality of the molds (**Figure 59**). Because the second coating has a strong odor, it is highly recommended to wear appropriate PPE.



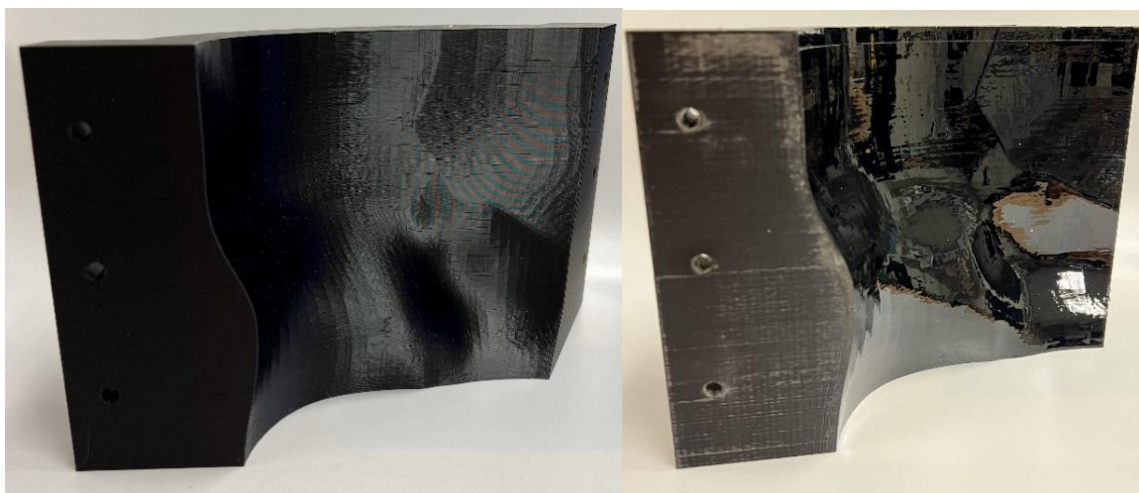


*Figure 59: A comparison of the 3D printed part without (left) and with (right) the XTC-3D finish.*

Additionally, heat inserts were installed on the three top mold pieces to facilitate the connection of the bone alignment device to the designed mold. These inserts ensure secure and precise alignment during the molding process, contributing to the overall accuracy and functionality of the final product.

## 4.5 SENSOR WIRING

Installing and wiring the sensors were critical steps in establishing accurate data collection and functionality of the silicone limb model. Proper soldering and cable management techniques were employed to secure and route the sensors correctly through the model.

All sensors were soldered and prepared for molding. Using a guide wire, the sensors were routed through the bone and into the designated location one at a time; this ensured that each sensor was placed exactly, minimizing the risk of damage or misalignment during the installation process.

The first step involved installing the sono ground crystals (crystals 1, 2, and 3 depicted in **Figure 60** below). These crystals were routed using a guide wire to establish precise placement. Once positioned, the crystals were tested in water to confirm their functionality before proceeding with the installation of other sensors.



*Figure 60: The sono ground crystals 1, 2, and 3 (highlighted by the red circles) were the first to be installed; these crystals were tested in water to confirm their functionality.*

After confirming the functionality of the ground crystals, the pressure sensors at the bottom of the limb were positioned in the distal femur bone model. This placement was necessary to obtain accurate pressure data from the distal end of the limb, which is crucial for comparing cases with and without the implant.

Next, the remaining sensors were routed through the limb. Starting from the bottom and working towards the top, each sensor was carefully threaded through its pre-determined path to certify that the cables did not interfere with sensor functionality or the model's structural integrity.

**Figure 61** below represents the completed wiring of the 16 pressure sensors and 12 sonomicrometry crystals.

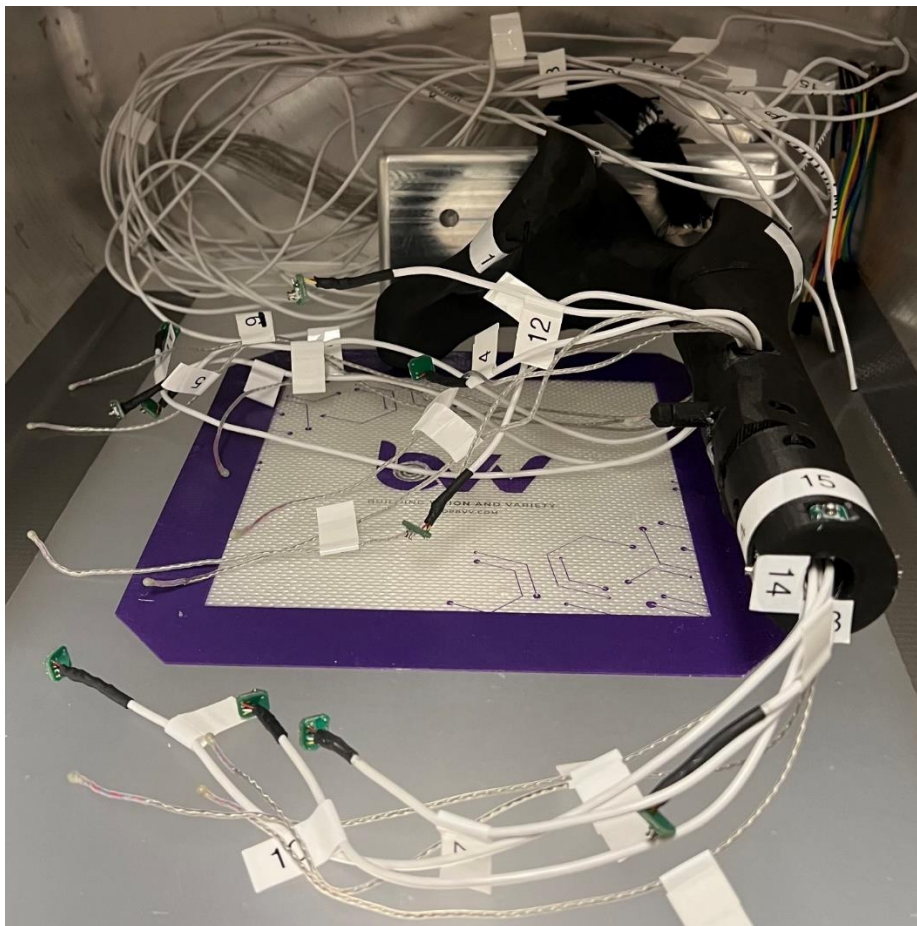


*Figure 61: The 16 pressure sensors and 12 sono crystals that were successfully routed through the molded bone.*

Effective cable management was vital during this phase. Proper routing and securing of the wires prevented movement or strain that could impact sensor performance. Cable ties and clips were used to secure the wires in place, ensuring they remained in their designated positions throughout the molding process.

By meticulously following these steps, the team certified that all sensors were accurately placed and securely routed, and thus, were ready for the final molding process. This thorough preparation was crucial for the successful operation of the sensorized silicone limb model.

These efforts ensured the sensors would provide reliable and accurate data during biomechanical testing, contributing to the project's success. The meticulous attention to detail in soldering, routing, and securing the sensors underscores the importance of precision in constructing complex models.

#### 4.6 SENSOR PRE-MOLDING

Prior to molding the limb, each pressure sensor and sono crystal was pre-molded to certify there were no air bubbles and to confirm functionality (**Figure 62**). This step was vital for verifying that the sensors were correctly angled and functioning as intended before the final molding process.

All wires were labeled on both sides to facilitate identification and proper connection. Before pre-molding, the sensors were cleaned with acetone to remove any oily residue, providing a clean surface for the silicone to adhere to.

The pre-molding process allowed for the sonomicrometry sensors to be angled properly, guaranteeing that their line of sight was not blocked by the wires. This precise angling was essential for accurate data collection.



*Figure 62: Pre-molded sonomicrometry and pressure sensors with the silicone poured into the molds.*

Pre-molding the sensors provided several advantages. First, it allowed for better control over the sensor angles, ensuring that they were positioned correctly within the limb. Additionally, pre-molding simplified the final molding process by creating a stencil to hold the sensors in place, making it easier to manage and pour the silicone.

By following these steps, the team verified that all sensors were properly angled, securely encased in silicone, and functioning correctly. This meticulous preparation was vital for the successful integration of the sensors into the final silicone limb model, ensuring reliable and accurate data collection during biomechanical testing. **Figure 63** below shows the result of pre-molding the sensors in silicone.



*Figure 63: The sensors encased in silicone prior to the final molding processes.*

## 4.7 FINAL MOLDING PROCESS

To ensure proper sensor alignment and adequate degassing of the silicone in the vacuum chamber, several key considerations were made during the final molding process. It was crucial not to pour more than 1500 grams of silicone at once to prevent air bubbles. Additionally, because the pre-molded sensors and sono crystals tended to float to the top of the silicone, a new molding process involving templates was designed to maintain accurate sensor positioning. The final limb required 10 pouring cycles, with a 4-hour curing period between each pouring cycle. **Figure 64** below illustrates the distinct levels of silicone poured.

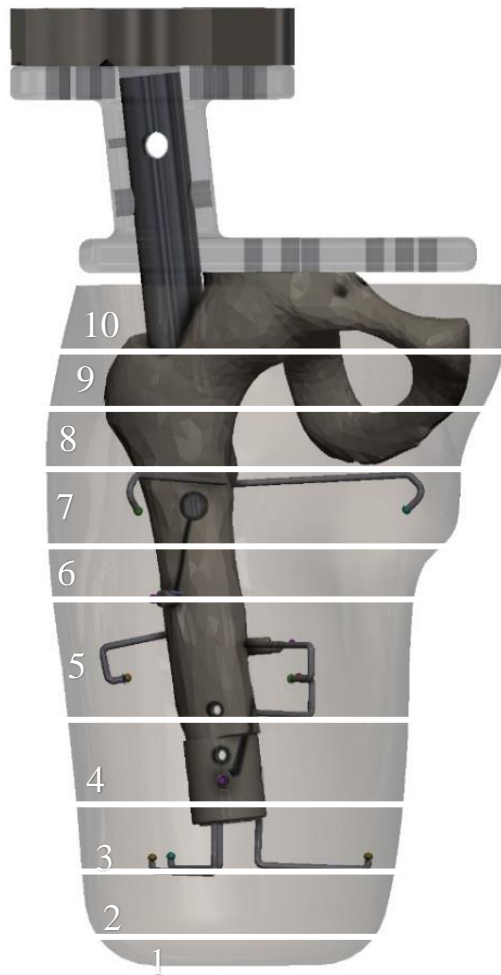


*Figure 64: The final molding of the limb was divided into 10 separate pours, selected based on component positioning and the maximum recommended amount of poured silicone.*

After validating sensor functionality, the final molding process began. All sensors, wires, and molds were cleaned with acetone to remove any oils that could inhibit silicone curing. From this point on, all components were handled exclusively with nitrile exam gloves. The first pour involved an initial 200 grams of silicone to ensure that no wires would touch the bottom of the limb, which can be seen in **Figure 65**.



*Figure 65: The initial 200-gram silicone pour preventing wires from sticking through the bottom of the limb.*

Using a stencil, the bottom level of sono crystals was placed in its designated location, and 300 grams of silicone was poured to secure the bottom half of the sensors without covering them entirely. The stencil was designed to match the inner contour of the limb, ensuring it was positioned at the correct level. **Figure 66** shows the stencil used for the bottom-level crystals. The pre-molded sensors' silicone blocks were placed in this stencil with the bottom half protruding, allowing the new silicone to bond with the bottom level of these blocks. After the 300-gram pour, the stencil was removed, leaving the sensors securely positioned.





*Figure 66: The stencil used to position crystals 7, 8, and 10 with their respective pressure sensors on the bottom level of the limb.*

The stencil in **Figure 66** was then removed, resulting in the configuration shown in **Figure 67** below. After this step, 600 grams of silicone was poured to cover the top of these sensors and the grounded crystal two and pressure sensors 3, 13, 14, 15, and 16.



*Figure 67: The first two levels of silicone with the bottom level of pressure sensors and sono crystals embedded.*

For the fourth pour, the stencil for the mid-level crystals, including crystals and pressure sensors 4, 6, and 12, was placed in the mold, and 1200 grams of silicone was poured (**Figure 68**).



*Figure 68: The removable template used to position sensors at the correct level, prepared for the 4th pour.*

Once the fourth pour was completed and cured, 600 grams of silicone was poured on top to cover the top level of these sensors (**Figure 69**).



*Figure 69: Mid-level sensors with silicone poured to the top of level 5 in preparation for level 6.*

This process continued with subsequent pours of 1000 grams, 300 grams, 1000 grams, 1250 grams, and 1000 grams of silicone to complete the molding process. Throughout the pouring cycles, careful attention was paid to cable location and sensor orientation. The result is depicted below in **Figure 70**, with a total of 7450 grams (7.45 kg) of silicone used.



*Figure 70: The final molding result with 7450 grams of cured silicone poured in ten sections.*

The demolding process required careful attention. To ensure that the silicone was binding well to itself, no mold release was used. This lack of mold release caused the silicone to adhere to the mold, making the demolding process challenging. **Figure 71** depicts the mold removal process. However, this process was still easier than working with the previous one-piece mold design.



*Figure 71: The demolding process, with the top sections removed first to avoid damaging the mold or silicone limbs.*

To demold the limb, all 21 screws were removed. Each mold piece was carefully pried off the molded limb using a flat head screwdriver, ensuring not to damage the mold or the silicone. This methodical approach preserved the integrity of the silicone limb and the embedded sensors remained intact throughout the process. **Figure 72** depicts the final sensorized silicone limb after the mold was removed. The red circles represent both the pressure sensor and the sonomicrometry crystal placed slightly below the pressure sensors.



*Figure 72: The final sensorized model limb with the KUKA attachment mounted. The red circles highlight the implanted pressure and sono crystals on this side of the limb.*

Key considerations when using Eco-Flex 00-31 Near Clear silicone include its 45-minute pot life, and a 4-hour cure time. Proper degassing requires reducing the silicone to -26 inches of mercury.

## 4.8 CONSTRUCTION DISCUSSION

The construction phase of the silicone limb model was a meticulous process that required careful planning, precise execution, and innovative problem-solving to achieve a high-quality final product. This section discusses the major aspects and challenges encountered during the construction process and the solutions employed to overcome them.

The KUKA attachment construction began with a design review and approval from my advisor, followed by 3D printing of a prototype for initial testing. This step was crucial for validating the part's alignment and geometry before finalizing the design. Sending the finalized design to SuNPe for manufacturing guaranteed a robust and exacting part, highlighting the importance of professional fabrication for critical components.

The model bone construction involved two key parts: the 3D-printed femur and pelvis, and the machined aluminum tube. Initially printed using PLA, the bone model failed stress testing, prompting a switch to onyx material on the Markforged 2 printer. This decision significantly improved the strength and durability of the printed parts. Adhering the parts together with 3M Scotch-Weld Plastic & Rubber Instant Adhesive PR40 and verifying their strength using the KUKA robot yielded a reliable model.

The mold construction process utilized extensive 3D printing with Eco ABS filament. To address the requirement for variable limb volumes, molds were printed with three different volumes: -10%, nominal, and +10%. This approach facilitated the study of limb volume effects on prosthetic socket fitment. The finishing process involved meticulous sanding and the application of XTC-3D to achieve a high-quality surface finish. Despite the challenges of the silicone adhering

to the mold, the multi-part mold design significantly improved ease of use compared to the one-piece mold.

The sensor wiring and installation were critical for certifying accurate data collection. Each sensor was carefully soldered, labeled, and routed through the bone using a guide wire. This process required meticulous attention to detail to prevent interference and ensure proper sensor alignment. Pre-molding the sensors allowed for precise angling and secure encapsulation, enhancing their performance in the final model.

The final molding process was designed to avoid air bubbles and ensure accurate sensor placement. Limiting the silicone pours to 1500 grams and using stencils for sensor alignment were two key strategies employed in this phase. The ten-pour process, with a four-hour curing time between pours, ensured the silicone bonded well and maintained the correct sensor positions. Despite the challenge of the silicone adhering to the mold, the multi-part design and careful demolding process ensured the integrity of the final product.

The construction phase successfully addressed major design concerns, validated parts through FEA, and ensured components were designed separately but integrated seamlessly. The use of professional manufacturing, advanced materials, and precise assembly techniques culminated in a robust, functional, and accurate silicone limb model. This phase highlighted the importance of detailed planning, thorough testing, and iterative improvements in achieving project goals.

## 5 VALIDATION

---

The validation phase is essential to confirm that the silicone limb model meets design specifications and performs as intended. This section covers several critical validation steps, including the evaluation of the silicone material, assessment of volume changes, and testing of integrated pressure sensors and sonomicrometry systems. These validation efforts ensure that the limb model accurately replicates human soft tissue behavior, maintains consistent performance across varying volumes, and provides reliable data through its sensor systems.

### 5.1 SILICONE VALIDATION

Modeling soft tissue is a complex task due to the variability in muscle and fat content, which affects limb stiffness. To address this challenge, the team reviewed data on suitable silicones for the project. While some companies have used ballistics gel, its limited shelf life made it impractical. Instead, the team selected the Smooth-On Ecoflex series for its durability and similarity to soft tissue. Based on published data, Ecoflex 00-31 was selected as the primary silicone due to its balance of stiffness and clarity [18]. In total, the team tested five different silicone stiffnesses, as depicted in **Figure 73** below.





*Figure 73: The various silicones tested for the limb from left to right: Dragon Skin 10, Ecoflex Gel 2, Ecoflex 00-20, Ecoflex 00-31 Near Clear, and Ecoflex 00-45 Near Clear.*

Dragon Skin 10 was too stiff to be used as a soft tissue model, though it could replicate skin well. Moreover, its 10-minute pot life was too short for the experiment. Ecoflex 00-45 was also too stiff but provided clearer results when molded.

Ecoflex Gel 2 and 00-20 were softer options with a 30-minute pot life, making them suitable candidates. However, Gel 2 remained too sticky even after curing, necessitating an additional coating for practical use. Based on these observations, Ecoflex 00-31 proved to be the most optimal choice, offering a 45-minute pot life, appropriate stiffness, and clarity for sensor visibility.

Given these results, the team decided to construct all limbs using Ecoflex 00-31 while also validating stiffness by building a softer limb using Ecoflex 00-20. This approach ensured a balance between realistic soft tissue modeling and practical application for sensor integration.

## 5.2 VOLUME CHANGE VALIDATION

To test the effects of volume change on prosthetic socket fitment, the team constructed the same limb with three different volumes. This approach was necessary because an amputee's limb volume can change multiple times throughout the day due to factors such as diet, weather conditions, comorbidities, and other variables. Research indicates that limb volume can fluctuate daily within a range of -11% to +11% [19]. The goal was to confirm that the magnetic attachment would work regardless of the limb volume at any given time.

Initially, the team considered creating silicone covers to increase the volume for testing. However, this approach was deemed inaccurate. To address this issue, the team decided to 3D print molds with three different inner volumes: -10%, nominal, and +10%. **Figure 74** below depicts these molds.



*Figure 74: The 3D printed molds with three different inner volumes: -10%, nominal, +10%.*

To validate that these limb molds were scaled properly, several factors were considered. First, it was crucial to select the origin for the scaling method. Initially, the top and bottom of the limb were chosen, but the results were unsatisfactory. After further analysis, the team decided to

scale the model limb with respect to the distal end of the femur; this location provided a more realistic representation of limb volume changes.

The STL part file was scaled to 0.966 for the -10% case and 1.0323 for the +10% case. This resulted in the following limb volumes:

- For the -10% case, the limb volume was 6389.79 cm<sup>3</sup>.
- For the nominal case, the volume was 7099.53 cm<sup>3</sup>.
- For the +10% case, the limb volume was 7809.94 cm<sup>3</sup>.

By accurately scaling the limb volumes, the team verified that the molds effectively represented the range of volume changes an amputee may experience. This validation was crucial for testing the magnetic attachment system, confirming its reliability across different limb volumes, and ensuring the prosthetic limb could accommodate daily fluctuations in limb size.

### 5.3 SONOMICROMETRY DEVICE CALIBRATION IN SILICONE

To certify that the correct speed of sound was utilized for the silicone, the team designed a calibration apparatus; said apparatus was used to validate the grounding method of the crystals and to calibrate the sonomicrometry device. This apparatus is depicted in the figure below. For this task, two sonomicrometry crystals were placed exactly 50 mm apart and grounded using the method explained in section 3.3.4.1.1. To calibrate the device, the speed of sound in the sonomicrometry software was adjusted until the final value for the distance between these crystals matched the 50 mm distance. The final speed of sound in Ecoflex 00-31 Near Clear was determined to be 1.032 mm/ $\mu$ s.



*Figure 75: The apparatus used to calibrate the sonomicrometry device to the Ecoflex 00-31 silicone.*

Similar devices were built to determine the maximum distance at which the sono crystals would function reliably. These tests confirmed that the maximum reliable distance between the crystals was 15 cm. This calibration process ensured that the sonomicrometry system provided accurate measurements and that the sensors were correctly positioned and functional within the limb model.

## 5.4 WATER TEST

To test the sonomicrometry crystal placement and confirm that the locations of the crystals would allow for proper triangulation of the limb, the team decided to first test the crystals in water (**Figure 76**); this allowed the team to validate the crystal placement geometry without needing to permanently mold 12 crystals in silicone. The task was accomplished by building a frame and subsequently attaching the 12 crystals.



*Figure 76: The sono water test model used to validate the crystal placement. Three crystals are grounded, and nine crystals are attached to their respective connectors, representing the wire length.*

The primary issue with the setup, depicted in **Figure 76**, was that all crystals were grounded to the frame, which did not allow validating the system's functionality during movement. The frame was constructed by attaching 3D-printed standoffs to designated locations on the bone cover.

The sonomicrometry device and the frame were then attached to the KUKA using the KUKA attachment mount, the aluminum tube, and the breakout box, as depicted in **Figure 77** below; this setup was lowered into a water bucket to begin the calibration.



*Figure 77: The sono water test experimental setup, including the breakout box and attachment, the KUKA attachment device, the model bone, and the aluminum tube and bone cover.*

The speed of sound varies depending on the temperature of the water. To calibrate this, two crystals were placed 75 mm apart, and the sonomicrometry speed of sound was adjusted to 1.59 mm/ $\mu$ s. This calibration ensured accurate measurements and validated the crystal placement for proper triangulation in the final silicone limb model.

Using this experimental setup, a few key tests were completed. First, the team wanted to determine if it was possible to localize the crystals and match the CAD crystal placement. For this task, the device had to be tuned for the various locations around the limb. **Figure 78** was obtained

by comparing the experimental locations with the SolidWorks positions on a 3D plot. In **Figure 78**, the blue circles represent the localized crystal locations using a trilateration technique.

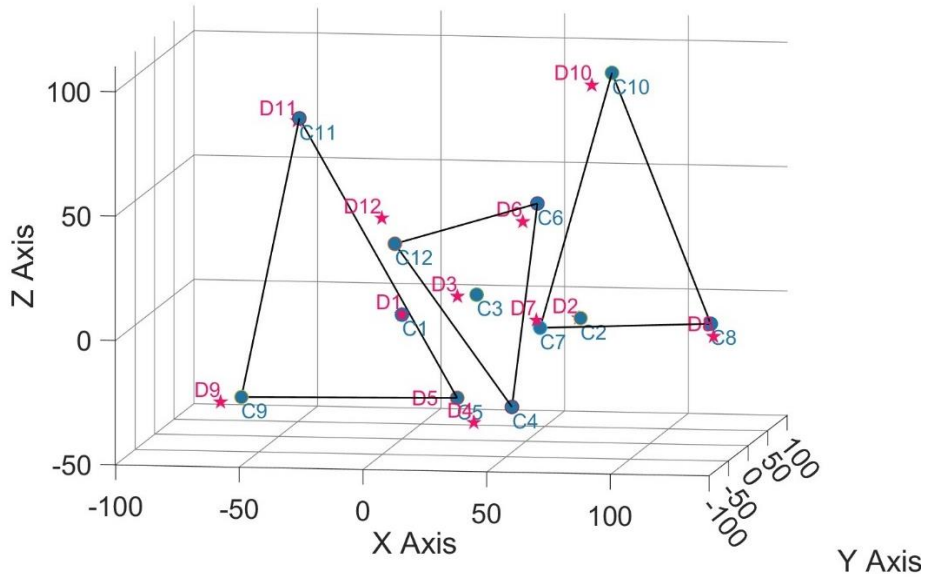


*Figure 78: The XYZ coordinates from the CAD (pink stars) plotted against the results from the sonomicrometry triangulation test in water (blue dots).*

Using these locations, the difference between the CAD position and the actual position was calculated. The crystals were mostly within 1 cm of their desired position, as shown in **Figure 79**.

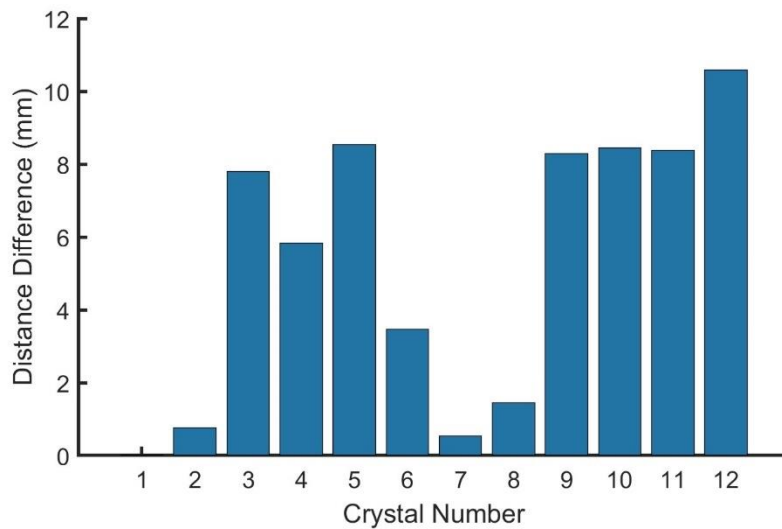


*Figure 79: The distance between the actual location and the designed location for each crystal.*

To further experiment with the water test, the team decided to move crystals 11, 5, and 9 respectively; these crystals were selected because they were positioned near the top of the water, allowing them to be moved without causing significant waves. The team utilized fishing wire attached to the crystals to minimize unintended water movement. **Figure 80** below illustrates the results obtained from the water test.

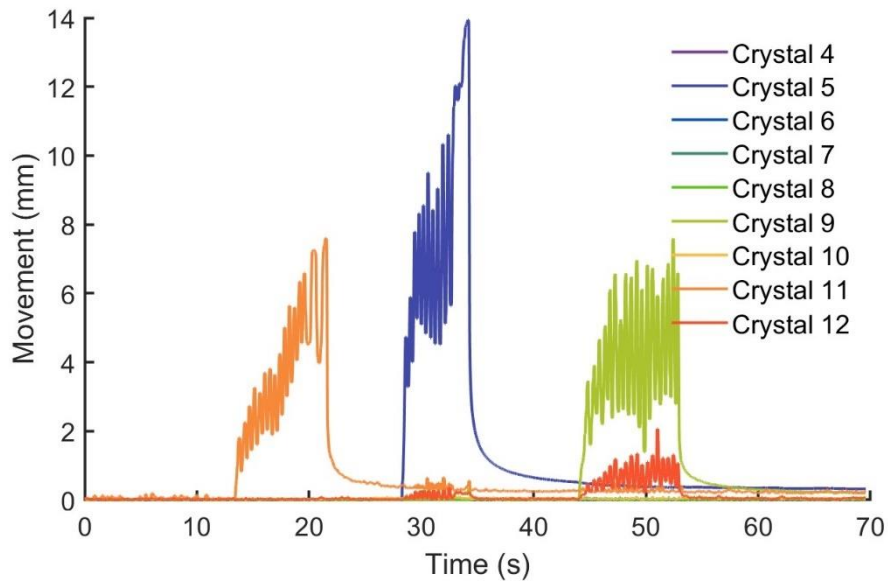


*Figure 80: The movement of crystals 11, 5, and 9.*

Crystal 11 moves first, reaching a maximum distance of 8 mm before returning to its original position. This is followed by crystal 5, which moves 14 mm before returning to its original position. Finally, crystal 9 moves a maximum distance of 8 mm, with a small wave causing crystal 12 to move 1 mm. This demonstrates the precision of the sonomicrometry device. To better illustrate the movement of these crystals, a close-up of the movement of crystal 11 is shown in **Figure 81** below.

To simulate realistic conditions, pressure was applied to these locations in an oscillating motion, mimicking the frequency of walking, which is approximately 0.8 Hz or 1.25 seconds/ step [20]. The crystals were pressed down repeatedly, with crystal 11 oscillating from 2 mm up to the



8 mm maximum distance in incremental steps. The same process was applied to crystals 5 and 9, ensuring that the testing conditions closely replicated the natural movements experienced during walking. This method provided a thorough validation of the sonomicrometry device's capability to accurately track and measure crystal movement within the limb model.

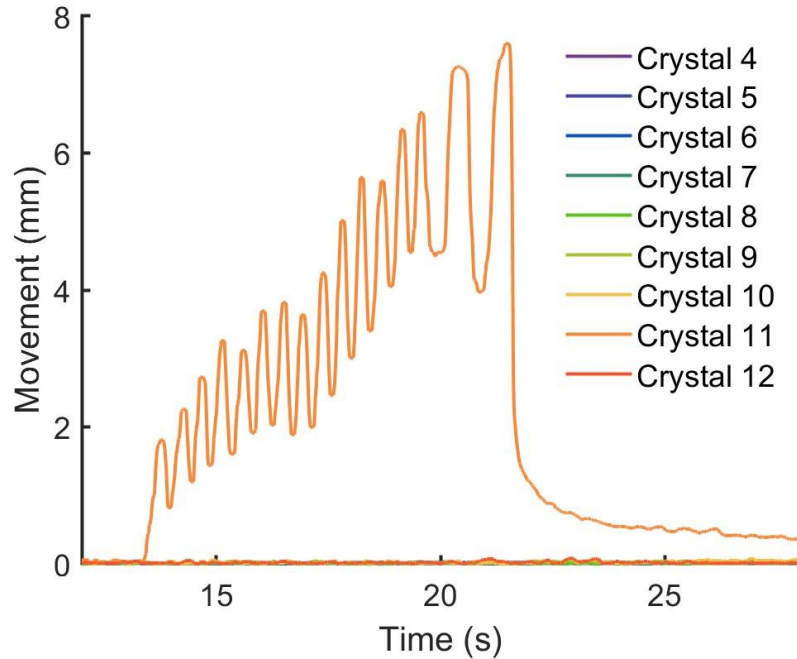


*Figure 81: A close-up of moving only crystal 11, showing the remaining crystals stationary with no movement.*

To calculate the positions of the remaining crystals, the team started with the three grounded crystals. Using the known XYZ coordinates of these grounded crystals (crystals 1, 2, and 3) and the distances between crystal 4 and each of these grounded crystals, the team localized the position of crystal 4. Specifically, the team used the distances between crystal 4 and crystals 1, 2, and 3, along with the coordinates of crystals 1, 2, and 3, to determine the XYZ coordinates of crystal 4.

Next, to determine the position of crystal 5, the team used the coordinates of crystals 1, 2, and 3, and the distances between crystal 5 and each of these grounded crystals; this provided the XYZ coordinates for crystal 5.

With the coordinates of crystals 1, 4, and 5 known, the team determined the position of crystal 7 using the distances between crystals 1, 4, and 5. Similarly, the position of crystal 9 was determined using the distances between crystal 9 and crystals 1, 4, and 5.

To localize crystal 8, the team used the coordinates of crystals 2, 3, and 4, along with the distances between crystal 8 and crystals 2, 3, and 4. For crystal 6, the coordinates of crystals 2, 4, and 8, and the distances between crystal 6 and crystals 2, 4, and 8 were used.

The coordinates of crystals 6, 7, and 8, and the distances between crystal 10 and crystals 6, 7, and 8 were used to localize crystal 10. Finally, for crystal 11, the coordinates of crystals 1, 6, and 9, and the distances between crystal 11 and crystals 1, 6, and 9 were used. Similarly, the position of crystal 12 was determined using the coordinates of crystals 1, 6, and 7, and the distances between crystal 12 and crystals 1, 6, and 7.

This systematic approach ensured an accurate determination of the XYZ coordinates for all the crystals, validating the effectiveness of the sonomicrometry system in tracking the positions of the crystals [21].

## 5.5 SONO & FINAL DEVICE VALIDATION

Following the water test, which validated the sonomicrometry crystal placement and triangulation technique, the team proceeded with the final construction of the limb in silicone. Once the limb was constructed, it was mounted on the KUKA robotic arm to achieve the project's overarching goal. **Figure 82** below depicts the sensorized model limb attached to the KUKA robotic arm.



*Figure 82: The final image with the sensorized model limb attached to the six-axis KUKA robotic arm.*

To attach the sensorized limb, the aluminum KUKA mount was first aligned with the two M5 alignment pins and then fastened using six M10 bolts. Next, the aluminum tube of the sensorized limb was placed in the KUKA mount and secured using two M10 shoulder bolts. Later,

three M6 screws were used to secure the bone cover to the KUKA mount. Lastly, four set screws were tightened to eliminate any tolerances in the parts.

It was crucial to ensure that the wires would not be strained during the KUKA's movement. The team meticulously planned the wire placement to avoid any interference with the robotic arm's path. The wires were routed to the side and up the robotic arm. **Figure 83** below provides a close-up view of the limb and breakout box mounted to the KUKA.

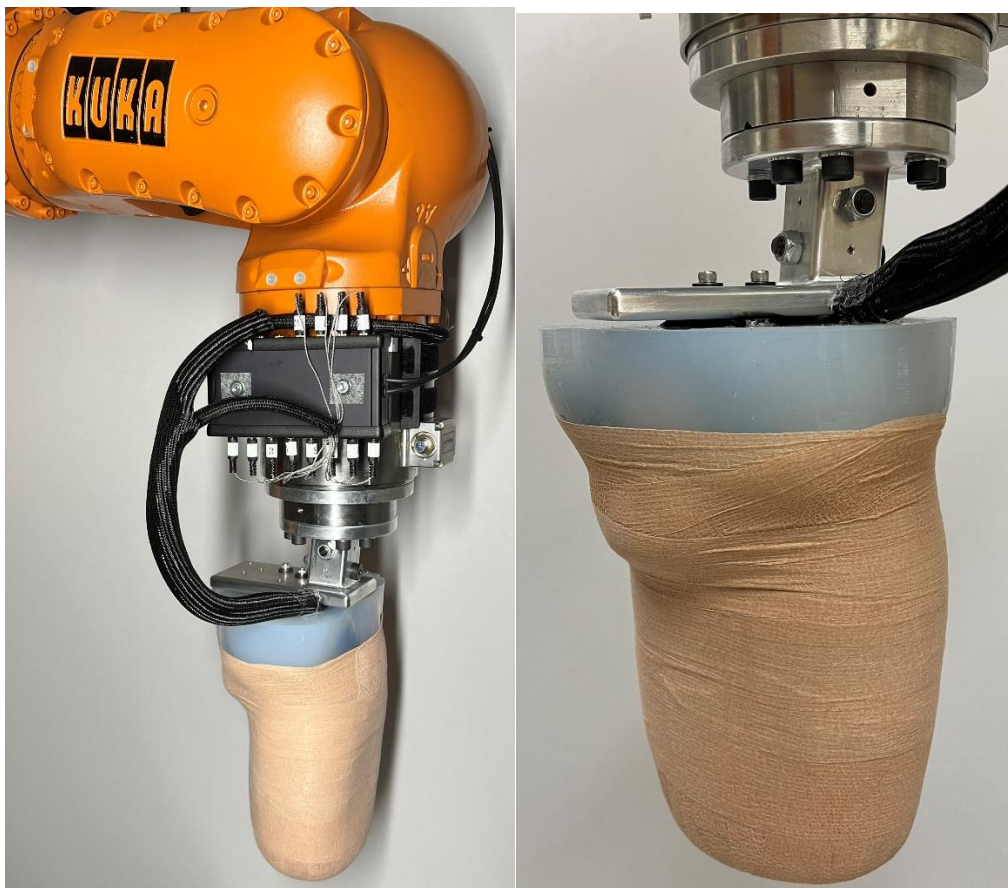


*Figure 83: A close-up view of the breakout box (left) and sensorized model limb (right) attached to the end effector of the KUKA robotic arm.*

Using the experimental setup in **Figure 83**, the team began to record and validate the device's functionality. It was essential to compare the results from the silicone model limb to the water test to ensure the quality of the limb matched the desired outcome. **Figure 84** below

depicts the triangulated silicone limb using the 12-channel sonomicrometry system, comparing the actual locations of the crystals (blue) with the intended locations from CAD (pink).

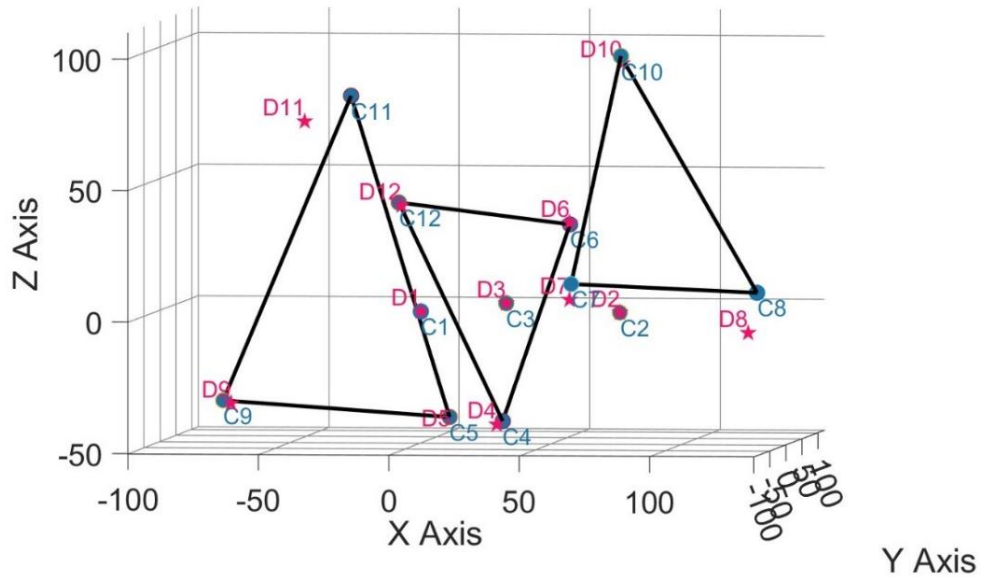


**Figure 84:** The XYZ coordinates from the CAD (pink stars) plotted against the results from the sonomicrometry triangulation test in silicone (blue dots) in 3D.

Comparing the crystal placement in silicone with the water test, it is evident that the crystals are placed more accurately. **Figure 85** shows the distance between the intended crystal location and the actual crystal location.

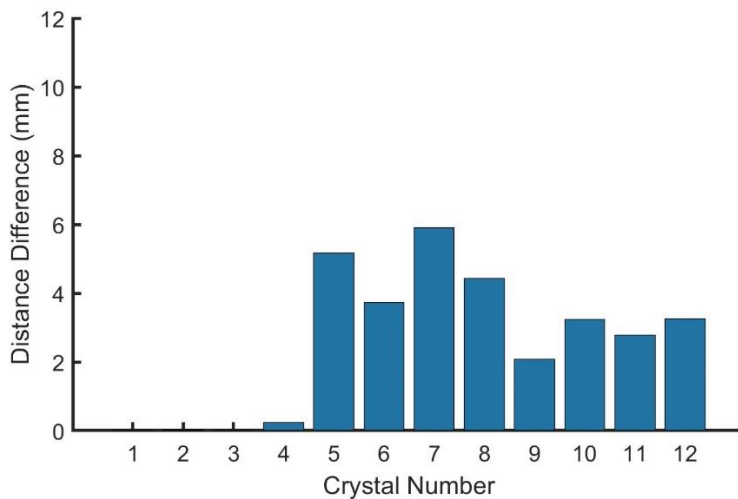


**Figure 85:** The distance between the actual location and the designed location for each crystal. The average difference is less than 5mm, which is remarkable considering the overall size of the limb.

The average distance between the actual crystal placement and the CAD crystal placement is less than 5mm, demonstrating that the molding method and stencil design accurately placed these crystals.

After validating the crystal placement, the team conducted experiments with the model limb. In one experiment, the team pressed the location of crystal 8 to verify if the limb was functioning as intended. When crystal 8 is pressed, the surrounding crystals also move since they are all embedded in the silicone limb. **Figure 86** below plots the movement of these crystals over time.

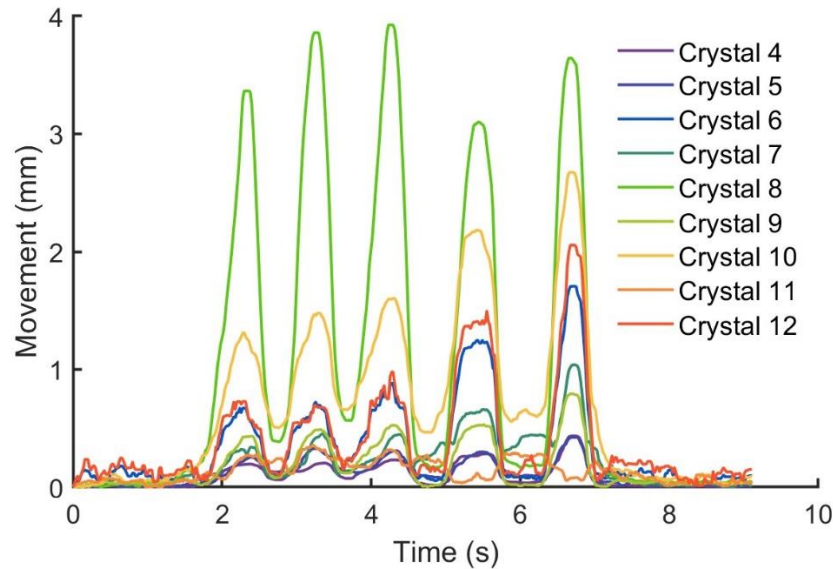


*Figure 86: The movement of crystals 4-12 in millimeters vs. time. In this experiment, only the location of crystal 8 was pressed.*

When crystal 8 is pressed, crystal 10, which is closest to it, experiences the second-largest movement; this is followed by crystal 12 and then crystal 6, which are on the same side of the limb as crystals 8 and 10. This demonstrates a major difference between the water and silicone tests. In the water test, when one crystal moves, only that crystal moves unless there is a wave, which subsequently moves the remaining crystals. In the case of silicone, the entire limb is interconnected, mimicking the behavior of soft tissue. Using this limb, the team can measure the

deformation of simulated tissue and validate the functionality of the prosthetic socket and the magnetic attachment method.

To further verify the limb's functionality and observe its behavior with a prosthetic socket, the team placed the limb inside the original mold to mimic a check socket for this experiment. A 25-pound weight was placed on top of the limb and removed three times. **Figure 87** shows the movement of these crystals during that experiment over time.

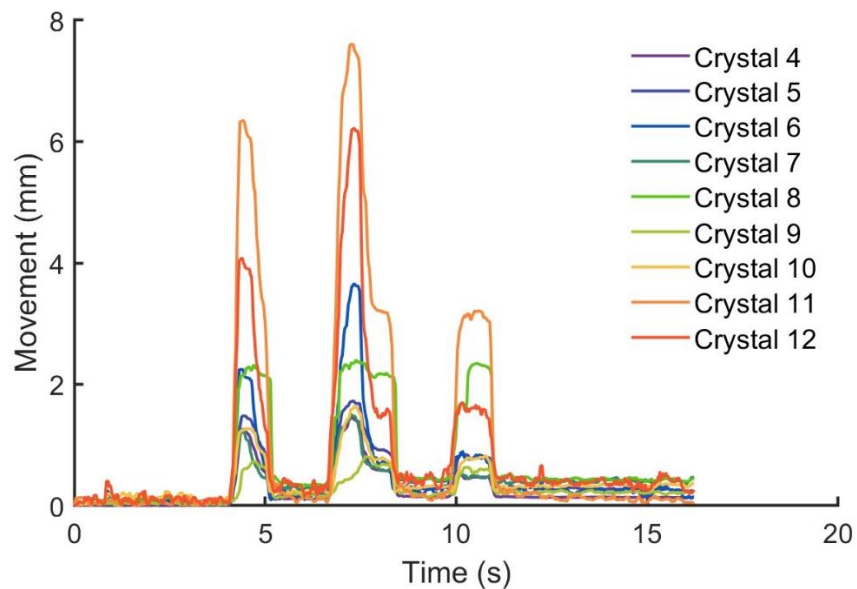


*Figure 87: The plot of movement in millimeters vs time when placing a 25-pound weight on top of the limb and removing it three times, indicated by the three distinct curves.*

It is evident that the 25-pound weight was not placed on the limb the same way each time. However, the crystal movement shows that the same crystals are experiencing the applied load similarly. Crystal 11, which is at the top of the limb closest to the location of the weight, experiences the maximum deformation, followed by crystal 12, which is below crystal 11 on the same side of the limb, and then crystal 8, also on the same side of the limb.

Based on the results from these experiments, it can be inferred that the limb is functioning as designed and is operating in a reliable manner.

## 5.6 PRESSURE SENSOR VALIDATION

The pressure and temperature sensors, along with the code to utilize them, were designed by another team member. I was involved in the construction and implementation of the silicone limb. To validate that these pressure sensors are working correctly, the team will report on the three most important ones, which include the pressure sensor located at the distal femur, greater trochanter, and ischial tuberosity. These tests were completed on all 16 pressure sensors to certify their functionality.

### 5.6.1 Distal Femur Pressure Sensor

It is crucial to measure the pressure at the distal femur to ensure that the end of the bone is not excessively loaded, which could cause pain for the amputee patient. To validate the distal femur pressure sensor, the end of the bone was pressed five times, and the pressure response was recorded over time (see **Figure 88** below).

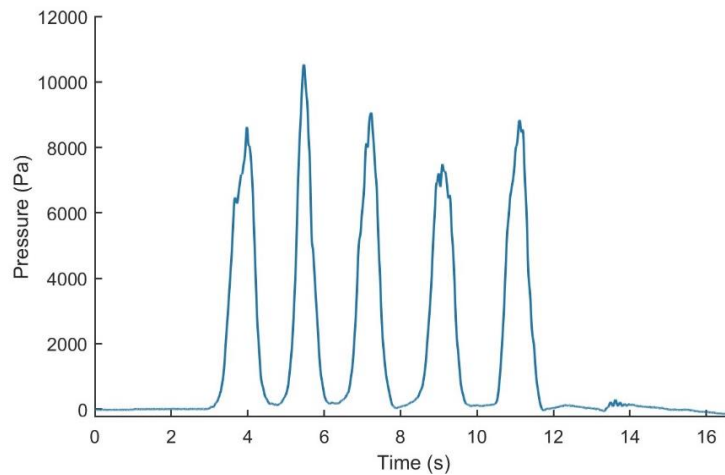


*Figure 88: The pressure vs. time plot of the distal femur created by pressing the end of the bone five times. The maximum recorded pressure was 10543.4 Pa.*

In transfemoral amputation, the residual limb cannot bear the body's weight directly on the transected end. Therefore, one of the primary goals of transfemoral amputation surgery is to



balance the muscles so that some weight can be borne on the sides of the thigh. For this reason, knowing the pressure at the bottom of the limb is important.

### 5.6.2 Greater Trochanter Pressure Sensor

The greater trochanter is a pressure-sensitive area, and it is important to ensure that the prosthetic socket is not applying excessive pressure to this bone, which could cause discomfort for the patient. Knowing the forces at this location is crucial for designing a comfortable and effective socket. The greater trochanter pressure sensor was tested by pressing and releasing the greater trochanter five times. The pressure response was recorded (see **Figure 89** below).

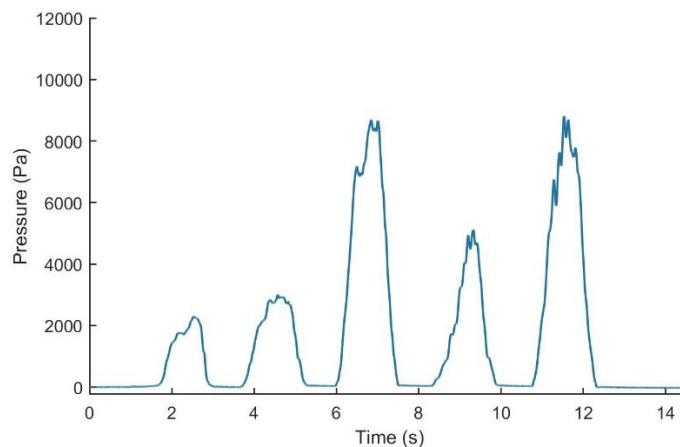


*Figure 89: The pressure at the greater trochanter created by pressing and releasing the greater trochanter five times. The maximum recorded pressure was 8507.9 Pa.*

### 5.6.3 Ischial Tuberosity Pressure Sensor

It is important to measure the pressure at the ischial tuberosity because it is used as a hard stop for ischial containment sockets. Instead of the end of the bone being loaded, the weight is distributed onto the ischial tuberosity, commonly known as the "sitting bone". The ischial tuberosity pressure sensor was validated by pressing and releasing this bony landmark five times. The pressure response was recorded each time and is depicted in **Figure 90** below.

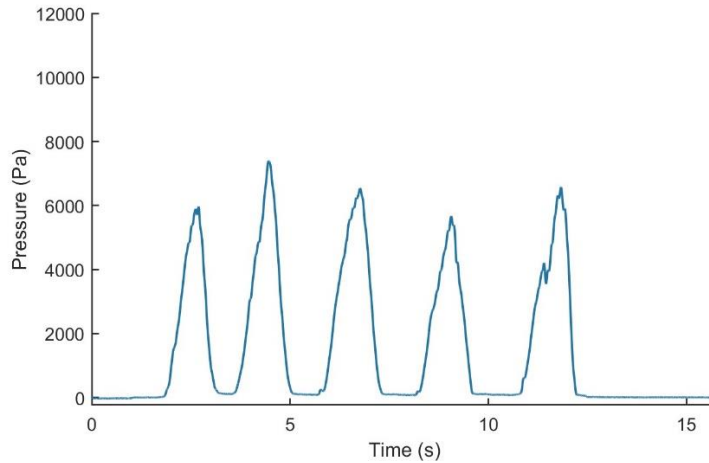


*Figure 90: The pressure at the ischial tuberosity created by pressing and releasing this bony landmark five times. The maximum recorded pressure was 7980.3 Pa.*

### 5.6.4 Temperature Measurement

The team also wanted to validate that the pressure sensors could provide temperature values. It is important to know the temperature at the bottom of the limb for the magnetic attachment portion of this project. During the pressure validation experiments, the temperature at the distal femur was recorded to verify that the temperature sensors were functioning correctly.

**Figure 91** below shows the results from this experiment.

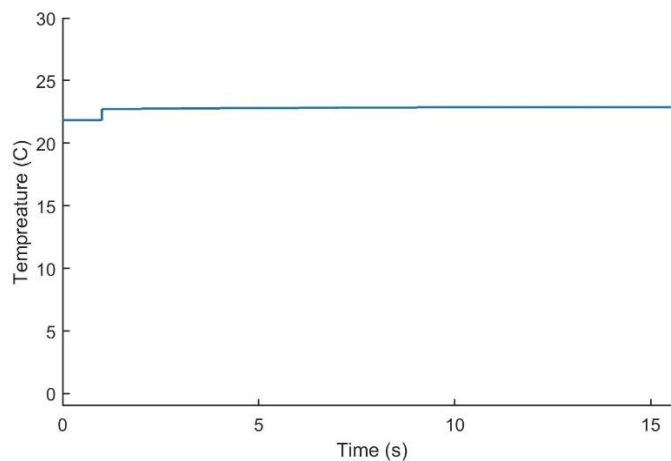


*Figure 91: The temperature of the distal femur recorded while completing the pressure experiment. The maximum recorded temperature was 22.2° Celsius.*

The plots depicted in the figure above demonstrate that the pressure sensors at key locations are responsive to applied forces and are functioning as intended. The temperature data further confirms that the sensors are operating correctly in their respective environments. To confirm the final pressure and temperature results, these sensors must be calibrated using a standardized calibration procedure.

## 5.7 VALIDATION DISCUSSION

The validation process was a critical phase in certifying that the sensorized silicone limb model met the rigorous standards required for accurate biomechanical analysis and practical application. The thorough validation covered multiple aspects, including silicone material selection, volume change impact, sonomicrometry, and pressure sensor functionality, each meticulously evaluated to confirm the model's reliability and effectiveness.

The selection of Smooth-On Ecoflex 00-31 silicone was pivotal. Extensive testing against other silicone types demonstrated that Ecoflex 00-31 provided an optimal balance of stiffness, transparency, and workability, closely mimicking the mechanical properties of human soft tissue. This material allowed for a realistic simulation environment where the sensor data could be reliably captured and analyzed.

Volume change validation was another crucial aspect. Given that an amputee's limb volume fluctuates throughout the day due to various factors, constructing limbs with -10%, nominal, and +10% volumes was necessary. The team designed and 3D printed molds to these specifications, ensuring that the limb models accurately reflected these volume changes.

The sonomicrometry validation was comprehensive, starting with the water test to ensure precise crystal placement and triangulation. The transition from water to silicone proved successful, with the average crystal placement accuracy within 5mm of the intended positions. This high level of precision validated the effectiveness of the molding method and stencil design. The experimental setup on the KUKA robotic arm further reinforced these findings, demonstrating consistent and reliable deformation measurements that closely matched the theoretical models.

Pressure sensor validation was equally rigorous. By focusing on key anatomical landmarks such as the greater trochanter, ischial tuberosity, and distal femur, the team ensured that the sensors provided accurate and meaningful data. The pressure sensors were critical for understanding how different parts of the limb bear weight and respond to external forces, directly impacting prosthetic socket design and patient comfort. The integration of temperature measurement capabilities added another layer of functionality, essential for monitoring conditions that could affect the magnetic attachment mechanism.

The final validation of the integrated system on the KUKA robotic arm was the culmination of these efforts. The precise attachment process, careful routing of wires, and detailed calibration of the sonomicrometry system ensured that the limb model functioned as intended. The experimental results, including the pressing and weight-bearing tests, demonstrated the model's ability to simulate real-world conditions accurately. The crystal movements under load confirmed the model's reliability in capturing tissue deformation and provided valuable insights for further refinement and application in prosthetic development.

In conclusion, the comprehensive validation process confirmed that the sensorized silicone limb model is a robust, accurate, and reliable tool for biomechanical analysis and prosthetic design. Each step, from material selection to final integration, was meticulously executed, ensuring that the model met all design goals and practical requirements. This validation not only establishes the model's credibility but also paves the way for its use in advanced prosthetic research and development, offering a promising future for improving amputee care and prosthetic technology.

## 6 CONCLUSION & FUTURE WORK

---

### 6.1 CONCLUSION

The development of the sensorized silicone limb model is the product of a comprehensive project dedicated to creating a reliable and functional tool for biomechanical analysis and prosthetic design. The final product demonstrates its ability to accurately simulate the mechanical properties of a transfemoral amputee limb, providing valuable data for improving prosthetic fit and function.

The total cost per limb without the ferromagnetic implant was \$1,720, while the cost for limbs with the implant was \$2,100; these costs include: \$1,320 for the sonomicrometry crystals (12 crystals at \$110 each), \$100 for various parts and fasteners, \$100 for the pressure sensors, and \$200 for the silicone. The careful selection of materials and components guaranteed that each limb model was both cost-effective and highly functional.

The final weight of the device was 17.4 pounds (7.89 kg), making it a realistic representation of a human limb in terms of weight distribution and balance. This weight is crucial for accurately simulating the forces and movements experienced by an amputee's residual limb during daily activities.

Throughout the validation process, the device consistently functioned as intended, accurately capturing pressure and temperature data, and providing reliable measurements of tissue deformation. The integration of the sensorized limb with the KUKA robotic arm further demonstrated the model's robustness and practical applicability, underscoring its value as a tool for advanced prosthetic research and development.

## 6.2 FUTURE WORK

Building on the success of this project, there are several areas for future work and improvement. One notable improvement is to refine the accuracy of the sensor data, particularly under dynamic conditions. Enhancing the calibration procedures for both the pressure sensors and sonomicrometry crystals will ensure even greater precision in data collection, thereby improving the model's reliability.

A pivotal next step is to collaborate with UCLA's Prosthetics and Orthotics Rehabilitation Center to create bespoke check sockets for limb models; these check sockets will enable rigorous testing of the model limbs with the KUKA robot, allowing for a more precise evaluation of the fit and functionality of the sockets under simulated real-world conditions. **Figure 92** shows the initial stages of crafting these check sockets, where the UCLA Prosthetics Center has created a limb positive of our model limb in preparation for building the check socket.



*Figure 92: The initial stages of making a check socket for the sensorized silicone limb model detailed in this report. The UCLA Prosthetics and Orthotics Center has created a limb positive of our model limb in preparation to build the check socket.*

By pursuing these future initiatives, the team aims to further improve the model's accuracy, functionality, and applicability. This ongoing development will contribute significantly to advancing prosthetic technology and enhancing the quality of life for amputees.



# 7 APPENDIX

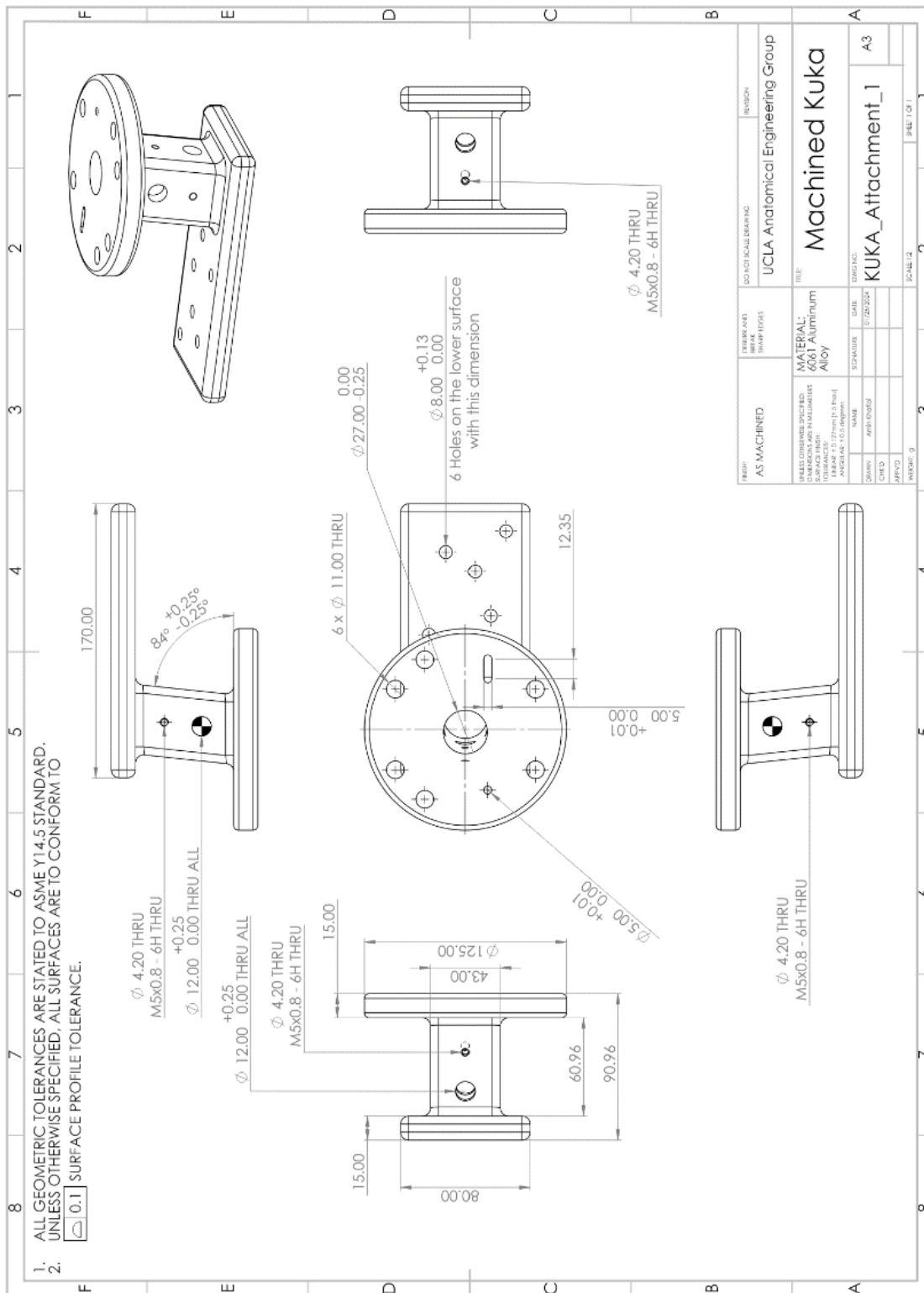


Figure 93: The KUKA Attachment device engineering drawing sent to SuNPc for machining.

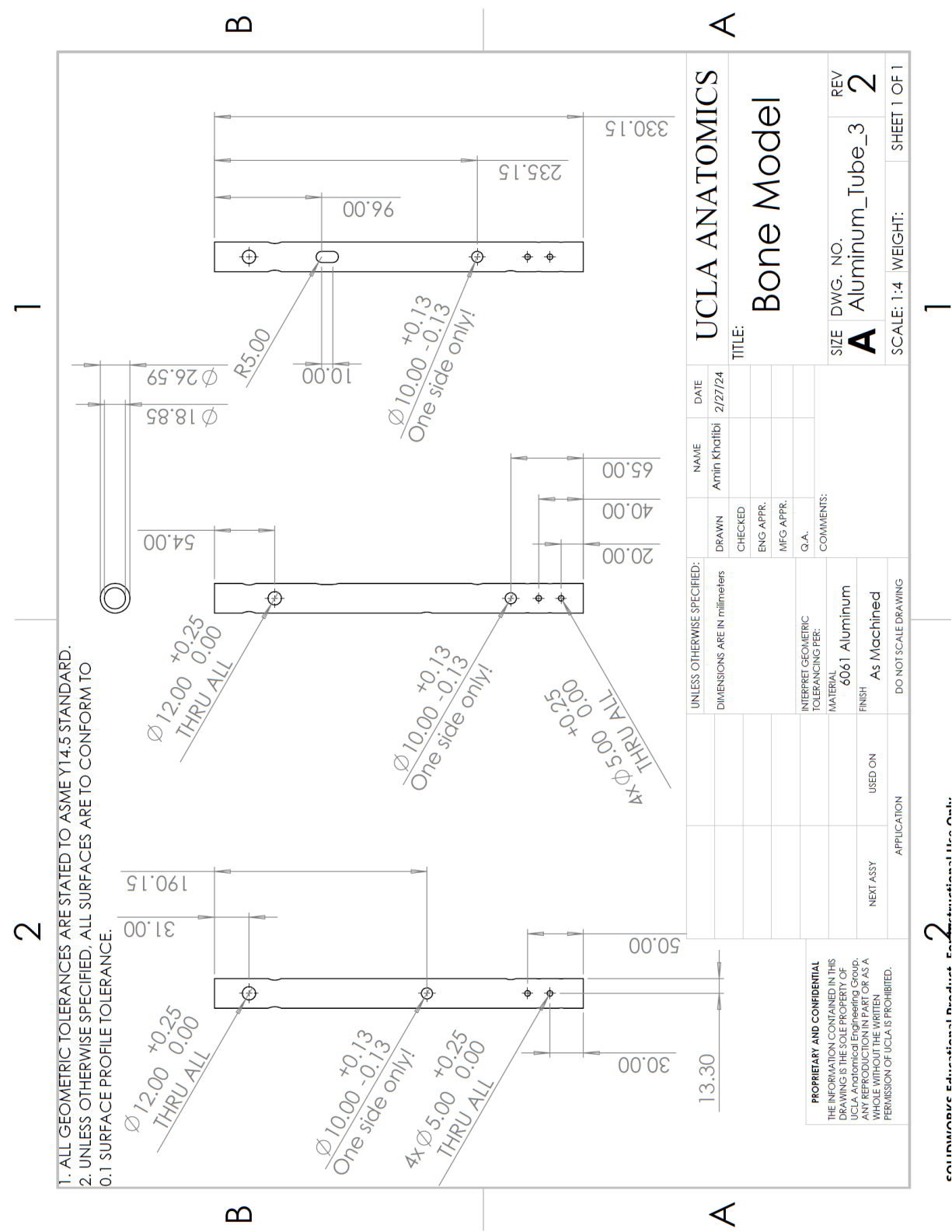
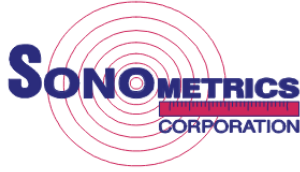


Figure 94: Engineering drawing of the aluminum tube used at UCLA machine shop to make the model.

*Table 1: The complete list of the parts and fasteners purchased from McMaster-Carr that were utilized to build one sensorized model limb. The total cost was \$94.75.*

<b>Part Name</b>	<b>Part Number</b>	<b>Quantity</b>	<b>Cost/part</b>	<b>Cost</b>
Alloy Steel Shoulder Screws, 12 mm Shoulder Diameter, 40 mm Shoulder Length, M10 x 1.5 mm Thread	92981a406	2	\$4.92/ pack of 4	\$2.46
General Purpose Zinc-Plated Steel Washer, Grade 5, for M10 Screw Size, 10.5 mm ID, 18.0 mm OD	98688A173	6	\$11.88/ Pack of 50	\$1.43
Fine-Thread Alloy Steel Socket Head Screw, M10 x 1.25 mm Thread, 40 mm Long	96144A265	6	\$8.18/ pack of 10	\$4.91
High-Strength Steel Nylon-Insert Locknut Class 10, Zinc Plated, M10 x 1.5 mm Thread, 10 mm High	94645a220	2	\$12.65/ pack of 25	\$1.02
Thick-Wall Aluminum Unthreaded Pipe 3/4 Pipe Size, 3 Feet Long	4559T212	1	\$115.17/ Pack of 2	\$57.59
Medium-Strength Steel Flange Nut-Class 8	90374A212	21	\$8.00/pack of 100	\$1.68
Steel Oversized Washer	94630A111	27	\$12.86/ pack of 50	\$6.95
Alloy Steel Socket Head Screw	91290A349	21	\$16.68/ pack of 25	\$14.02
Heat-Set Inserts for Plastic	94459A220	6	\$14.93/ pack of 25	\$3.58
Zinc-Plated Alloy Steel Socket Head Screw	90128A266	6	\$9.20/ pack of 50	\$1.11



QUOTE # IN000004537

Date: October 17, 2023

500 Nottinghill Road  
 London, ON N6K 3P1  
 CANADA

Phone +1 (519) 474-6464  
 Fax +1 (519) 474-6426

University of California at  
 Los Angeles  
 Dept of Mechanical and  
 Aerospace Engineering  
 Los Angeles, CA 90095

Attn: Dr. Tyler Clites

Reference - P.O. #	CIP	Salesperson	Ship Via	Terms Code
	London, ON	WS		N30

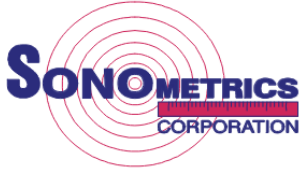
Item No.	Description/Comments	Quantity	U/M	Unit Price	Amount
DS3-TRX-12-USB	12 Channel Sonomicrometer Digital sonomicrometer hardware with USB Interface 12 Transceiver (TRX) channels 4 A/D input channels SonoSOFT software suite (SonoLAB, SonoView and SonoDCU) 12 um measurement resolution All cables required to setup system	1	EA	\$15,700.00	\$15,700.00
DISCOUNT	Discount Amount Received from Rental Payments Prior to Purchase.	1	EA	(\$1,000.00)	(\$1,000.00)
S&H PRIO	Shipping & Handling (Priority) Via FedEx International	1	EA	\$300.00	\$300.00

**Terms:**

All prices in U.S. dollars. This quote is valid for 30 days.  
 Please note that applicable duties and taxes must be paid by the recipient.  
 Payment due within 30 days of invoice with a penalty of 2% interest, per month on  
 overdue accounts. Delivery will be confirmed upon acceptance of order. Please  
 make all checks payable to Sonometrics Corporation. If you have any questions  
 regarding this quotation, please contact Sonometrics at +1 519 474-6464

Subtotal before taxes	\$15,000.00
Total taxes	\$0.00
Total amount	\$15,000.00
Amount due (USD)	\$15,000.00

Figure 95: The SonoMetrics Quote for the 12 channel sonomicrometer.



QUOTE # IN000004536

Date: October 12, 2023

500 Nottinghill Road  
London, ON N6K 3P1  
CANADA

Phone +1 (519) 474-6464  
Fax +1 (519) 474-6426

University of California at  
Los Angeles  
Dept of Mechanical and  
Aerospace Engineering  
Los Angeles, CA 90095  
  
Attn: Dr. Tyler Clites

Reference - P.O. #	CIP	Salesperson	Ship Via	Terms Code
	London, ON	WS		N30

Item No.	Description/Comments	Quantity	U/M	Unit Price	Amount
BOB-12CH	Break Out Box - 12 Channel 12-channel break-out box for use with TRX box. Includes 12 foot extender cable & inverter switch for each channel	1	EA	\$650.00	\$650.00
2R-36T-40-NS	2mm Transducer Silastic Tubing 2mm round, silastic tubing of 40 inch length, no intro, stereo connector (pricing includes discount based on quote of 50+ order)	8	EA	\$106.25	\$850.00
S&H PRIO	Shipping & Handling (Priority) Via FedEx International	1	EA	\$90.00	\$90.00

**Terms:**

All prices in U.S. dollars. This quote is valid for 30 days.  
Please note that applicable duties and taxes must be paid by the recipient.  
Payment due within 30 days of invoice with a penalty of 2% interest, per month on overdue accounts. Delivery will be confirmed upon acceptance of order. Please make all checks payable to Sonometrics Corporation. If you have any questions regarding this quotation, please contact Sonometrics at +1 519 474-6464

Subtotal before taxes	\$1,590.00
Total taxes	\$0.00
Total amount	\$1,590.00
Amount due (USD)	\$1,590.00

Figure 96: The SonoMetrics quote for the breakout box and eight 2mm transducer on silastic tubing.







# Prototypes Quotation

Quotation No.: SP21FA003-20240126A

Client No.: SP21FA003  
 Client: [University of California, Los Angeles](#)  
 Tel.:  
 Fax.:  
 Contact:  
 Website:  
 E-mail:

Provider: SUNPE PROTOTYPE(HK) CO., LIMITED  
 Address: No.70 Tongxing Xi Rd,Dongsheng Town,  
 Zhongshan City, Guangdong, 528414, P.R.China  
 Tel.: +86-18022182683  
 Fax.: +86 (0) 760 22211992  
 Contact: Cherry Luo  
<http://www.sunpe.com>  
 E-mail: [sales\\_31@sunpe.com](mailto:sales_31@sunpe.com)

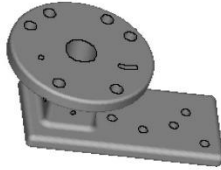
	Machined Kuka	Aluminum 6061-T6	CNC	1	USD 500
 <p> <b>Size:</b>            Max X:202.500 mm            Max Y:125.000 mm            Max Z:90.960 mm    <b>Volume:423974 mm3</b>              After treatment: As machined         </p>					

Figure 99: The prototyping quote from SuNPe for the KUKA attachment device.



## 8 REFERENCES

---

- [1] A. Eshraghi, N. Osman, H. Gholizadeh, M. Karimi and S. Ali, "Pistoning assessment in lower limb prosthetic sockets.," *Prosthetics and Orthotics International.*, vol. 36, no. 1, pp. 15-24, 2012.
- [2] W. Flanagan, K. becraft, H. Warren, A. stavrakis, N. Bernthal, T. Hardin and T. Clites, "Prosthetic Limb Attachment via Electromagnetic Attraction Through a Closed Skin Envelope," *IEEE Transactions on Biomedical Engineering*, vol. 71, no. 5, pp. 1552-1564, 2022.
- [3] K. L. Moore, A. F. Dalley and A. M. Agur, *Clinically Oriented Anatomy*, Wolters Kluwer, 2017.
- [4] E. J. Strauss, S. J. Nho and B. T. Kelly, "Greater trochanteric pain syndrome," *Sports Medicine and Arthroscopy Review*, vol. 18, no. 2, pp. 113-119, 2010.
- [5] P. contributors, "Lower Limb Prosthetic Sockets and Suspension Systems," Physiopedia, 1 August 2022. [Online]. Available: [https://www.physio-  
pedia.com/index.php?title=Lower\\_Limb\\_Prosthetic\\_Sockets\\_and\\_Suspension\\_Systems&  
oldid=312786](https://www.physio-<br/>pedia.com/index.php?title=Lower_Limb_Prosthetic_Sockets_and_Suspension_Systems&<br/>oldid=312786). [Accessed 28 March 2023].
- [6] E. S. Neumann, J. S. Wong and R. L. Drollinger, "Concepts of Pressure in an Ischial Containment Socket: Measurement," *Journal of Prosthetics and Orthotics*, vol. 17, no. 1, pp. 2-11, 2005.
- [7] S. Turner, A. Belsi and A. H. McGregor, "Issues faced by people with amputation(s) during lower limb prosthetic rehabilitation: A thematic analysis," *Prosthetics and Orthotics International*, vol. 46, no. 1, pp. 61-67, 2022.

- [8] V. S. Lee, S. E. Solomonidis and W. D. Spence, "Stump-socket interface pressure as an aid to socket design in prostheses for trans-femoral amputees—a preliminary study," *Proceedings of the institution of Mechanical Engineers*, vol. 211, no. 2, pp. 167-180, 1997.
- [9] C. Lee, "Intertrochanteric Fracture Short Nail," Caseclips, 2023.
- [10] B.-J. Park, H. m. Cho, K.-Y. An and H. Lee, "Acute Arterial Occlusion Following Primary Total Knee Arthroplasty.," *Knee surgery & related research.*, vol. 30, pp. 84-88, 2018.
- [11] R. A. Shanto, M. Khalil, S. Z. Sultana, E. Z. Epsi, S. K. Bose, M. S. Latif, R. Siddiquee, M. T. Russel and S. A. Sumi, "Variation of Mid shaft Antero-posterior and Transverse Diameter of Femur in Bangladeshi People.," *Mymensingh Med J.*, vol. 33, no. 1, pp. 234-238, 2024.
- [12] SonoMetrics Corporation, "Sonomicrometry - How it works," SonoMetrics Corporation, [Online]. Available: [https://www.sonometrics.com/sono\\_101.htm](https://www.sonometrics.com/sono_101.htm).
- [13] Markforged, "Material Datasheet Composites," 10 10 2023. [Online]. Available: <https://s3.amazonaws.com/mf.product.doc.images/Datasheets/Material+Datasheets/CompositesMaterialDatasheet.pdf>.
- [14] D. J. Miligan, S. O'Brian, D. Bennett, J. C. Hill and D. E. Beverland, "The effects of age and gender on the diameter of the femoral canal in patients who undergo total hip replacement," *Bone Joint Journal*, vol. 95, no. 3, pp. 339-342, 2013.
- [15] F. A. Appoldt, L. Bennett and R. Contini, "Tangential pressure measurements in above-knee suction sockets," *Bulletin of Prosthetics Research*, vol. 10, no. 13, pp. 70-86, 1970.

- [16] S.-T. Ko, F. Asplund and B. Zeybek, "A Scoping Review of Pressure Measurements in Prosthetic Sockets of Transfemoral Amputees during Ambulation: Key Considerations for Sensor Design," *Sensors*, vol. 21, no. 15, 2021.
- [17] D. S. Drummonds, R. G. Narechania, A. N. Rosenthal, A. L. Breed, T. A. Lange and D. K. Drummond, "A study of pressure distributions measured during balanced and unbalanced sitting," *Journal of Bone and Joint Surgery*, vol. 64, no. 7, pp. 1034-1039, 1982.
- [18] J. L. Sparks, N. . A. Vavalle, K. E. Kasting, B. Long and M. L. Tanaka, "Use of Silicone Materials to Simulate Tissue Biomechanics as Related to Deep Tissue Injury," *ADVANCES IN SKIN & WOUND CARE*, vol. 28, no. 2, pp. 59-68, 2015.
- [19] L. Paternò, M. Ibrahimi, E. Rosini, . G. Menfi, . V. Monaco, E. Gruppioni, L. Ricotti and A. Menciassi , "Residual limb volume fluctuations in transfemoral amputees," *Scientific Reports*, vol. 11, 2021.
- [20] P. Heinemann and M. Kasperski, "Damping Induced by Walking and Running," *Procedia Engineering*, pp. 2823-2831, 2017.
- [21] J. Smitherman, "Mathematics," 24 October 2018. [Online]. Available: <https://math.stackexchange.com/questions/2969363/finding-a-4th-point-in-3d-space-knowing-3-other-points-and-2-distances-to-the-4t>.